Reliable Multi-Point Transmissions Over Directional MISO TWDP Fading Channels

Stefan Schwarz [ID], *Senior Member, IEEE*, and Markus Rupp [ID], *Fellow, IEEE*

Abstract—**In this paper, we consider wireless transmissions over directional multiple-input single-output (MISO) two wave with diffuse power (TWDP) fading channels, subject to interference over the same type of channel. TWDP fading is known to exhibit an outage behavior that can be even worse than Rayleigh fading and has experimentally been observed in a number of vehicular channel measurement campaigns. To enhance the reliability of multi-point transmissions over MISO TWDP fading channels, we propose a zero-forcing based coordinated beamforming scheme, for which we can analytically characterize and optimize the outage probability of the multi-point transmissions. Based on the developed outage expressions, we furthermore propose a greedy coordinated scheduling approach that attempts to maximize the achievable rate of the system. Finally, we propose a transmission rate adaptation scheme for fixed size packet transmissions, which supports reliable and at the same time resource efficient multi-point transmissions.**

Index Terms—**Beamforming, scheduling, rate adaptation, two wave with diffuse power fading, reliability, outage probability.**

I. INTRODUCTION

MOBILE wireless communication systems have long been pure best-effort services, which are, as such, not able to guarantee a demanded level of link reliability. Best-effort services are not a suitable foundation for many critical applications, such as, road-safety related vehicular communications [1], [2]. In the standardization of fifth generation (5G) and beyond mobile communication systems, this drawback has been recognized and many efforts have been made to enable ultra reliable low latency communications (URLLC); e.g., [3]–[6]. However, this turned out to be a challenging task, which is not entirely resolved at the present time [7]. Different applications demand different levels of link reliability. For example, for non-critical applications as supported in fourth generation (4G) long term evolution (LTE), the packet transmission success probability lies in the order of 99 %, whereas for saftey-critical applications, e.g., in the context of vehicular communications, the success probability must be as high as 99.99 999 % [8].

In mobile wireless communications, the spatial density of concurrently active and thereby interfering links is continuously increasing. Novel concepts, such as, machine to machine (M2M) and vehicle to everything (V2X) communications, as well as, innovative technologies, such as, distributed massive multiple-input multiple-output (MIMO) [9] and dynamic distributed antenna systems (dDASs) [10], cell-free massive MIMO [11], [12], transmissions in the millimeter wave (mmWave) band [13], [14], and non-orthogonal multiple access (NOMA) [15], [16], are contributing to this trend. In such dense scenarios, the interference between simultaneously active links has a significant impact on the reliability of the transmissions. In most cases it is hard to impossible to analytically evaluate the outage behavior of the system, since the probability distribution of the signal to interference and noise ratio (SINR) of a communication link can often not be characterized analytically. Then, however, it is not possible to guarantee a certain level of link reliability of the system. One remedy is interference coordination, e.g., utilizing coordinated scheduling or beamforming techniques [17]–[19], which can alleviate inter-link interference when accurate channel state information at the transmitter (CSIT) is available and thereby facilitate an analytic link outage characterization.

In late 4G standards (release 13 and above), full-dimension massive MIMO has been introduced and further enhanced during 5G standardization [20]. Thereby two-dimensional antenna arrays are utilized at least on one link-end (commonly, for space-reasons, at the base station/infrastructure node) to provide a directional view of the wireless channel and to enable three-dimensional beamforming; i.e., the antenna arrays allow to resolve the multipath profile of the channel in the angular (elevation and azimuth) domain and to steer beams along preferred directions. Correspondingly, directional channel models, such as, the third generation partnership project (3GPP) three-dimensional channel model [21], [22] or the Quadriga channel model [23], became relevant for the optimization of wireless communication systems. These channel models are powerful tools that are well-suited for generating realistic random realizations of commonly encountered propagation environments, e.g., for rural/urban outdoor/indoor scenarios, and are therefore indispensable for system evaluation. Yet, they suffer from relatively high computational complexity and do not facilitate analytical insights or optimizations.

In many situations, especially for higher carrier frequencies such as mmWaves, the most relevant channel fading characteristics can be captured by much simpler models. Under line of sight

(LOS) conditions, for example, it is often sufficient to account for a single strong so-called specular component of the channel plus a Rayleigh fading component that accounts for diffuse background scattering. More accurate models take into account two strong specular components, in order to model multipath interference effects [24]. The applicability of such models for vehicular communications has been demonstrated experimentally by measurements and ray-tracing simulations of vehicle to vehicle (V2V) and vehicle to infrastructure (V2I) scenarios [25], [26]. When we consider transmit and receive beamforming on top of a propagation channel that is dominated by two strong specular components, the effective single-input single-output (SISO) channel of a link, including the transmit/receive beamformers, can be well modeled as TWDP fading [27].

The TWDP fading model is known for its potentially worse-than-Rayleigh fading behavior in terms of signal outage probability [28], [29], caused by destructive interference of the two specular components. It is therefore important to account for this type of fading, when designing a reliable communication system. Notice that Rice and Rayleigh fading are special cases of TWDP fading and are therefore also covered by such a system design. The performance of transmissions over TWDP fading channels has been investigated in a number of publications: In [30], the authors investigated the bit-error ratio performance of BPSK transmissions over TWDP fading channels, including maximum ratio combining (MRC) of multiple independent branches. In [31], the authors derived the outage probability of cooperative relay networks under TWDP fading, and, in [32], the author conducted a capacity analysis of TWDP fading channels. In [33], the authors derived analytic expressions for the average probability of successful energy detection based spectrum sensing over TWDP fading channels. In [27], we investigated the outage probability of transmissions over TWDP fading channels that are subject to multi-point interference over TWDP fading channels; the provided outage expressions, however, require multi-dimensional numeric integration and are therefore practically not useful.

The mmWave band has been considered as a viable candidate for vehicular communications already in the 1980 s in the railroad context [34]. Yet, the main interest was sparked with the development of the IEEE 802.11ad standard operating at 60 GHz [35], which has also led to integrating mmWave V2X into the 3GPP 5G standard [36]. There are a number of reasons for this development: First and probably foremost is the large bandwidth available in the mmWave bands, which allows for a massive exchange of sensing data amongst vehicles [37], to support, e.g., collision avoidance in high-level autonomous/automated driving [38]. Secondly, short symbol durations, as enabled by large bandwidths in mmWave systems, support ultra-low latency communications [39], which is important for safety-critical information exchange amongst vehicles. Furthermore, narrow antenna radiation beams, which are necessary to compensate for the high pathloss in the mmWave band, allow for high spatial connection densities thanks to spatial reuse [40]. Lastly, mmWaves are also suitable for radar applications, thus supporting joint communication and radar systems [41].

Contribution: In this paper, our focus is on supporting reliable multi-point V2I communications. We consider transmitters (infrastructure nodes) that are equipped with antenna arrays and receivers (vehicles) that feature a single (directional) receive antenna, i.e., MISO transmissions per link. Our focus is on transmissions in the mmWave band, where the effective directional channel can be well modeled as TWDP fading. We consider multiple concurrently active and interfering communication links and propose coordinated beamforming and scheduling techniques to enhance the reliability and outage performance of the system. We account for imperfect CSIT due to movement of the receivers and/or scatterers in the environment. Thereby, our main underlying assumption is that the transmitters are able to keep track of the macroscopic channel properties of the two dominant scattering multipath components, namely, their pathloss and mean azimuth/elevation angle of departure. However, the relative phase-variations of these two multipath components are too fast, such that the transmitter does not know if the transmitted signal interferes constructively or destructively at the receivers. This is a reasonable assumption for mmWave transmissions in mobile scenarios, as the signal phases change significantly even for small movements in the order of millimeters. This random/unknown phase assumption ultimately leads to TWDP fading of the effective SISO channels (including transmit/receive beamformers), which significantly impairs the outage performance of the communication links. We propose a coordinated beamforming scheme, based on zero-forcing, that facilitates an analytic calculation of the outage probability of the links. Specifically, under the proposed beamforming scheme, the outage probability is dictated by TWDP fading of the intended signal and by the probability distribution of a sum of Rayleigh fading interference terms; it is therefore hard to characterize in closed-form. We propose an iterative, asymptotically tight bounding algorithm for the outage probability, which facilitates an outage-based optimization of the parameters of the proposed beamforming scheme. We, furthermore, propose a greedy coordinated scheduling method for grouping of concurrently active links, with the goal of maximizing the achievable rate of the system. Finally, we propose reliable and resource efficient transmission rate adaptation methods for the considered multi-point TWDP fading scenario, assuming transmission of fixed size packets. The present paper is an extension of our conference paper [42], where we considered only single-point (interference-free) transmissions.

In previous work, robust beamforming strategies for MISO interference channels with uncertain CSIT have been developed, e.g., in [43]–[46]. These methods have in common that they either follow a chance-constrained robust design principle, where the authors consider a probabilistic outage constraint on the SINR for a given distribution of the CSIT error, or a worst-case approach, where the authors maximize the worst-case SINR under a norm constraint on the CSIT error. In all of these contributions, an additive CSIT uncertainty of the form $\mathbf{h} = \hat{\mathbf{h}} + \mathbf{e}$ is assumed, where $\hat{\mathbf{h}}$ is the estimated CSIT and $\mathbf{e}$ is an estimation error. In this work, however, we consider a model of the form $\mathbf{h} = \hat{\mathbf{h}}_1 e^{j\varphi_1} + \hat{\mathbf{h}}_2 e^{j\varphi_2} + \mathbf{e}$, where not only the additive error $\mathbf{e}$ is unknown, but additionally also the phases φ_1, φ_2 of the two

dominant scattering multipath components are unknown by the transmitter; hence, existing robust beamforming approaches are not applicable in our case.

To summarize, this paper contains the following main contributions:

- We propose robust outage optimized beamforming strategies for MISO multi-point transmissions over TWDP fading channels with imperfect CSIT.
- We consider CSIT assumptions that are suitable for mmWave transmissions in mobile scenarios, where the transmitters (infrastructure nodes) are equipped with antenna arrays and the receivers are equipped with single directional receive antennas. For such situations it has been shown by measurements that TWDP fading is suitable to characterize the fading of the effective channels (including the spatial filtering effects of the directional receive antennas) [25], [26], [47]. Our assumptions on CSIT uncertainty go beyond a simple additive error model.
- We propose methods to analytically characterize the outage performance of MISO multi-point transmissions over TWDP fading channels under the proposed zero-forcing beamforming strategy.
- Based on this outage characterization, we develop methods for multi-point scheduling and transmission rate adaptation to support reliable communication links.

Organization: In Section II, we discuss the employed directional MISO channel model and our assumptions on CSIT. We then show how this model leads to TWDP fading of the effective SISO channel and extend the model to multi-point transmissions, accounting for inter-link interference. In Section III, we discuss the proposed enhancements to enable reliable multi-point transmissions over directional MISO TWDP fading channels. We propose a beamforming coordination scheme that facilitates an analytic calculation and optimization of the link outage probability in Section III-A. We then propose a link scheduling coordination algorithm that enables the maximization of the transmission rate of the system, while accounting for the link outage probability in Section III-B. Finally, we propose a transmission rate selection method that supports resource efficient transmission of data packets at non-zero link outage probability in Section III-C. We conduct simulations to evaluate the performance of the proposed techniques in Section IV and we conclude the paper in Section V.

Notation: We denote vectors and matrices by bold lower and upper case letters, $\mathbf{x}$ and $\mathbf{X}$ resp., and sets by calligraphic letters $\mathcal{X}$. The modulus and argument of a complex number z are $|z|$ and $\arg(z)$. The size of set $\mathcal{X}$ is $|\mathcal{X}|$. The Frobenius norm of matrix $\mathbf{X}$ is $\|\mathbf{X}\|$ and the conjugate-transpose is $\mathbf{X}^H$. The left null space of tall matrix $\mathbf{X} \in \mathbb{C}^{n \times m}$ is $\text{null}(\mathbf{X}) = \{\mathbf{x} \in \mathbb{C}^{n \times 1} | \mathbf{X}^H \mathbf{x} = \mathbf{0}\}$ and the m-dimensional subspace spanned by $\mathbf{X}$ is $\text{span}(\mathbf{X})$. The principal eigenvector of matrix $\mathbf{X}$ is $\max \text{eigvec } \mathbf{X}$. The complex Gaussian distribution with mean vector $\boldsymbol{\mu}$ and covariance matrix $\mathbf{C}$ is $\mathcal{CN}(\boldsymbol{\mu}, \mathbf{C})$. We denote closed intervals as $[a, b]$ and open intervals as (a, b). The uniform distribution on the interval (a, b) is $\mathcal{U}(a, b)$ and the chi-square distribution with two degrees of freedom is χ_2^2. The expected value of random variable r is $\mathbb{E}(r)$ and the probability of random event a is $\mathbb{P}(a)$.

II. SYSTEM MODEL

In this paper, we consider downlink V2I multi-point transmissions, where the transmitters (infrastructure nodes) are equipped with antenna arrays and the receivers (vehicles) are equipped with single receive antennas. Our focus is on transmissions in the mmWave band, where the multipath channel between transmitter and receiver can be characterized by a few scattering components, as has been observed in many measurement campaigns [48]–[51]. Furthermore, we assume that the receivers utilize directional antennas to compensate for the large pathloss experienced in the mmWave band. In Section II-A, we describe the corresponding adopted directional MISO channel model. Then, in Section II-B, we discuss our assumptions on CSIT. In Section II-C, we show how this leads to TWDP fading of each transmission link, and, in Section II-D, we characterize the SINR of multi-point transmissions over directional TWDP fading channels.

A. Channel Model

We consider for each link a MISO directional cluster-ray channel model [52]

$$\mathbf{h} = \sum_{c=1}^{N_c} \alpha_c e^{-j\varphi_c} \sum_{r=1}^{R_c} \mathbf{h}_{r,c} + \mathbf{h}_d, \quad \mathbf{h}_c = \sum_{r=1}^{R_c} \mathbf{h}_{r,c}, \quad (1)$$

$$\mathbf{h}_{r,c} = \Delta\alpha_{r,c} e^{j\Delta\varphi_{r,c}} \mathbf{a}_t \left(\boldsymbol{\Psi}_c + \boldsymbol{\Delta\Psi}_{r,c} \right) g \left(\boldsymbol{\Xi}_c + \boldsymbol{\Delta\Xi}_{r,c} \right). \quad (2)$$

Here, N_c denotes the number of scattering clusters and α_c is the mean macroscopic pathloss of cluster c, determined by the propagation distance and the directional receive antenna gain. Parameter φ_c is the mean macroscopic phase-shift of cluster c, caused by the propagation delay, and $\boldsymbol{\Psi}_c = (\theta_c, \phi_c)$ is the mean angle of departure as seen by the transmitter, with θ_c denoting the elevation angle and ϕ_c the azimuth. Similarly, $\boldsymbol{\Xi}_c$ is the mean angle of arrival as seen by the receiver.

Each cluster is composed of a number R_c of scattering rays. $\Delta\alpha_{r,c}, \Delta\varphi_{r,c}$ are ray-specific variations of the pathloss and the phase-shift around their respective mean values, caused by the electromagnetic properties of the scattering object. Similarly, $\boldsymbol{\Delta\Psi}_{r,c}, \boldsymbol{\Delta\Xi}_{r,c}$ are ray-specific variations of the angles, which are in most cases negligible, since the distance between transmitter/receiver and scatterer is commonly large compared to the dimensions of the scattering object.

Vector $\mathbf{a}_t(\boldsymbol{\Psi}) \in \mathbb{C}^{N_t \times 1}$ is the array response of the transmit antenna array, with N_t denoting the number of transmit antennas, and $g(\boldsymbol{\Xi}_c) \in \mathbb{C}$ is the angle dependent gain of the receive antenna. Vector $\mathbf{h}_c$ represents the sum over all rays within a cluster and vector $\mathbf{h}_d \sim \mathcal{CN}(\mathbf{0}, 2\sigma_h^2 \mathbf{I}_{N_t})$ is a diffuse background scattering component. The setup is illustrated in Fig. 1.

In the following, we restrict to $N_c = 2$ dominant scattering clusters. It is well-known that mmWave channels exhibit a sparse multipath profile [53]. When we consider the effective channel including the directional receive antenna with fixed pointing direction (e.g., pointing along the driving direction of the vehicle), it has been shown in measurements that a restriction to $N_c = 2$ is well justified for mmWave transmissions [24], [25], [47], [51]. This is because the directional receive antenna
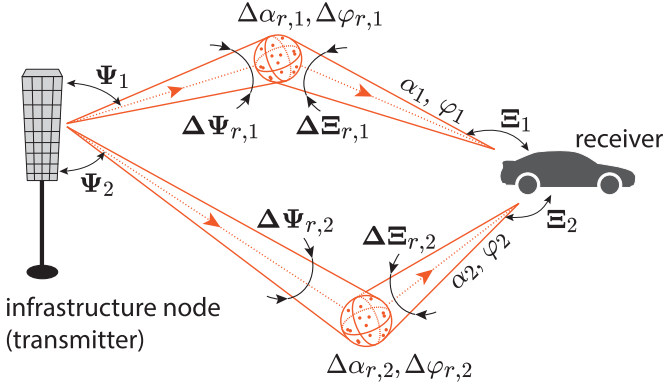
Fig. 1. Illustration of the considered directional MISO cluster-ray channel model with two dominant clusters. The infrastructure node (transmitter) is equipped with an antenna array providing a directional view of the channel, the receiver is equipped with a single active (directional) antenna.

acts as a spatial filter that effectively reduces the already sparse mmWave multipath propagation environment to one (typically, the line-of-sight) or two (an additional non-line-of-sight) dominant paths.

We do not account for the propagation delay time difference between the two clusters, which would lead to frequency-selectivity of the channel. The reason for this is that we have a multicarrier system in mind, where the subcarrier bandwidth is too small to resolve the temporal delay difference [52]. To simplify notations, we focus on a single frequency-flat subcarrier in this paper and omit a subcarrier index.

To summarize, we consider a two-path MISO directional channel model according to

$$\mathbf{h} = \alpha_1 e^{-\mathrm{j}\varphi_1}\mathbf{h}_1 + \alpha_2 e^{-\mathrm{j}\varphi_2}\mathbf{h}_2 + \mathbf{h}_d, \qquad (3)$$

where $\mathbf{h}_1$ and $\mathbf{h}_2$ are directional channel components and $\mathbf{h}_d$ is a diffuse Rayleigh fading channel component. Measurements have shown that the diffuse Rayleigh fading component is commonly relatively weak compared to the directional components; yet, it is not negligible [24], [25], [47], [51].

B. CSIT Estimation Model

We consider two distinct scales for the temporal/spatial variations of the considered channel model:
1) We consider *fast relative inter-cluster phase-variations* of the two dominant clusters. Specifically, we assume that the phase difference $\varphi_1 - \varphi_2$ between these two clusters varies quickly with the movement of the receiver/scatterers. This is reasonable, since the two clusters be observed from two entirely different angular directions, such that their sum causes a fading pattern that varies significantly over very short distances (within fractions of the carrier wavelength, i.e., millimeters).
2) Compared to the inter-cluster phase variations, we consider *slow relative intra-cluster phase-variations*. That is, we assume that the temporal/spatial scale over which the intra-cluster phase-differences $\Delta\varphi_{r,c} - \Delta\varphi_{k,c}, \forall r, k$ of each cluster vary significantly is large compared to

the temporal/spatial scale over which the inter-cluster phase difference $\varphi_1 - \varphi_2$ changes significantly. This is reasonable, because the intra-cluster angular-spread $\max_r \Delta\boldsymbol{\Psi}_{r,c} - \min_r \Delta\boldsymbol{\Psi}_{r,c}$ is small compared to the inter-cluster angle difference, as illustrated in Fig. 1. Combined with the assumption that the pathloss variations $\Delta\alpha_{r,c}$ also change slowly, this leads to slow variations of each cluster's channel vector $\mathbf{h}_c$, compared to the temporal/spatial scale over which their sum $\alpha_1 e^{-\mathrm{j}\varphi_1}\mathbf{h}_1 + \alpha_2 e^{-\mathrm{j}\varphi_2}\mathbf{h}_2$ varies significantly.

From these two temporal/distance scales we deduce the following two assumptions about CSIT:
1) We assume that the transmitter has no valid information about the phases φ_c, since they vary too quickly. Hence, for the transmitter $\varphi_c \sim \mathcal{U}(0, 2\pi)$ holds. The transmitter does also not know $\mathbf{h}_d$, only its variance σ_h^2.
2) We assume that the transmitter has knowledge about the channel vectors $\mathbf{h}_c$ and the pathloss values α_c of each cluster. This CSIT can be estimated during the uplink transmission and is (at least approximately) still valid during downlink transmission, provided the duplex time interval is sufficiently short. CSIT estimation errors can be taken into account by the diffuse component $\mathbf{h}_d$.

These CSIT assumptions lead to two types of uncertainty that the transmitter has to deal with: 1) Uncertainty about the fading state of the diffuse channel $\mathbf{h}_d$. 2) Uncertainty about the multi-path interference state of the two dominant scattering components $\mathbf{h}_1$ and $\mathbf{h}_2$; i.e., the transmitter does not know whether signals transmitted over these two components will add-up constructively or destructively at the receiver, due to their unknown phase relationship. The former uncertainty is a common assumption in literature and many prior contributions have dealt with this type of uncertainty, e.g., [43]–[46]. Yet, to the best of the authors' knowledge, no robust beamforming schemes for the latter type of uncertainty exist so far.

C. Effective SISO Channel Model Including Beamforming

The transmitter applies beamformer $\mathbf{f} \in \mathbb{C}^{N_t \times 1}$ for data transmission. This converts the MISO channel into an effective SISO channel including the beamformer

$$h = \mathbf{h}^{\mathrm{H}}\mathbf{f} = \alpha_1 e^{\mathrm{j}\varphi_1}\mathbf{h}_1^{\mathrm{H}}\mathbf{f} + \alpha_2 e^{\mathrm{j}\varphi_2}\mathbf{h}_2^{\mathrm{H}}\mathbf{f} + \mathbf{h}_d^{\mathrm{H}}\mathbf{f}$$
$$= V_1 e^{\mathrm{j}\psi_1} + V_2 e^{\mathrm{j}\psi_2} + z_d, \qquad (4)$$
$$V_c = \alpha_c \left|\mathbf{h}_c^{\mathrm{H}}\mathbf{f}\right|, \quad \psi_c = \varphi_c + \arg\left(\mathbf{h}_c^{\mathrm{H}}\mathbf{f}\right) \sim \mathcal{U}(0, 2\pi), \qquad (5)$$
$$z_d \sim \mathcal{CN}\left(0, 2\sigma_d^2\right), \ \sigma_d^2 = \sigma_h^2 P, \qquad (6)$$

where $P = \|\mathbf{f}\|^2$ denotes the transmit power. For fixed amplitudes V_1, V_2, the probability distribution of the absolute value of the effective SISO channel $|h|$ follows the TWDP fading model. More generally, if ψ_c follows any arbitrary probability distribution (not necessarily uniform), $|h|$ follows the generalized two ray (GTR) fading model [54] (TWDP is a special case of GTR, also known as GTR-uniform). We assume $\varphi_c \sim \mathcal{U}(0, 2\pi)$ and thus $\psi_c \sim \mathcal{U}(0, 2\pi)$ in this paper, as this is the most reasonable assumption for our scenario, as argued in Setion II-B. However,

we would like to mention that the proposed solutions can also be applied under GTR fading with arbitrary phase distribution, simply by replacing the cumulative distribution function (cdf) of TWDP fading in our expressions by the corresponding cdf of GTR fading.

TWDP fading is commonly characterized by the following three parameters

$$\Omega = V_1^2 + V_2^2 + 2\sigma_d^2, \tag{7}$$

$$K = \frac{V_1^2 + V_2^2}{2\sigma_d^2}, \quad \Delta = \frac{2V_1V_2}{V_1^2 + V_2^2}, \tag{8}$$

where Ω is the mean receive power. The K-factor quantifies the relative power of the two specular components V_1, V_2 w.r.t. the diffuse component z_d. The Δ-parameter quantifies the relative strength of the two specular components w.r.t. each other. Notice, for $\Delta = 0$, TWDP fading reduces to Rice fading and for $K = 0$ it reduces to Rayleigh fading.

D. Multi-Point Transmissions

We now consider multiple transmitter-receiver pairs (links) that are simultaneously active. To account for this, we add transmitter-receiver link indices to our previous notation. The input-output relationship of user u served by transmitter u is

$$y_u = \mathbf{h}_u^H \mathbf{f}_u x_u + \sum_{j \in \mathcal{S}_g \setminus \{u\}} \mathbf{h}_{u,j}^H \mathbf{f}_j x_j + n_u, \tag{9}$$

$$\mathbf{h}_u = \sum_{c=1}^2 \alpha_{c,u} e^{-j\varphi_{c,u}} \mathbf{h}_{c,u} + \mathbf{h}_{d,u}, \tag{10}$$

$$\mathbf{h}_{u,j} = \sum_{c=1}^2 \alpha_{c,u,j} e^{-j\varphi_{c,u,j}} \mathbf{h}_{c,u,j} + \mathbf{h}_{d,u,j}. \tag{11}$$

Here, $\mathbf{h}_u$ and $\mathbf{f}_u$ denote the channel and beamformer of the intended link u, x_u is the corresponding unit-power information symbol, and $n_u \sim \mathcal{CN}(0, 2\sigma_n^2)$ denotes the receiver noise of user u. Vector $\mathbf{h}_{u,j}$ denotes the interference channel of user u with respect to link j and $\mathbf{f}_j$ is the corresponding beamformer. Set $\mathcal{S}_g \subseteq \{1, \ldots, N_u\}$, $u \in \mathcal{S}_g$ is the group of transmitter-receiver pairs that are simultaneously active with link u, and N_u is the total number of considered transmitter-receiver pairs.

The total set of links $\{1, \ldots, N_u\}$ is split by scheduling coordination into a number of N_s distinct simultaneously active groups $\mathcal{S}_\ell$, such that, $\cup_{\ell=1}^{N_s} \mathcal{S}_\ell = \{1, \ldots, N_u\}$ and $\mathcal{S}_\ell \cap \mathcal{S}_k = \emptyset, \forall \ell \neq k$. Different groups are served at orthogonal time-frequency resources, as further discussed in Section III-B.

1) Effective Multi-Point Channel Model: The effective channels $h_{u,j} = \mathbf{h}_{u,j}^H \mathbf{f}_j$ follow a model similar to (4)

$$h_{u,j} = V_{1,u,j} e^{j\psi_{1,u,j}} + V_{2,u,j} e^{j\psi_{2,u,j}} + z_{d,u,j}, \tag{12}$$

$$V_{c,u,j} = \alpha_{c,u,j} \left| \mathbf{h}_{c,u,j}^H \mathbf{f}_j \right|, \quad \psi_{c,u,j} \sim \mathcal{U}(0, 2\pi), \tag{13}$$

$$z_{d,u,j} \sim \mathcal{CN}\left(0, 2\sigma_{d,u,j}^2\right), \quad \sigma_{d,u,j}^2 = \sigma_{h,u,j}^2 P_j. \tag{14}$$

Here, $\alpha_{c,u,j}$ and $\mathbf{h}_{c,u,j}$ are the gain and channel vector of cluster c of the interference channel between transmitter j and user u,

$\sigma_{h,u,j}^2$ is the variance of the associated diffuse channel component and P_j is the transmit power of link j. For the effective channel $h_u = \mathbf{h}_u^H \mathbf{f}_u$, we just use a single index, as in $V_{c,u}$, $\sigma_{d,u}^2$ and $\psi_{c,u}$. Thus, the absolute value of each of the links $|h_{u,j}|$ follows TWDP fading statistics.

The instantaneous SINR of user u is

$$\beta_u = \frac{\left| \sum_{c=1}^2 V_{c,u} e^{j\psi_{c,u}} + z_{d,u} \right|^2}{2\sigma_n^2 + \sum_{j \in \mathcal{S}_g \setminus \{u\}} \left| \sum_{c=1}^2 V_{c,u,j} e^{j\psi_{c,u,j}} + z_{d,u,j} \right|^2}. \tag{15}$$

The probability distribution of β_u is dictated by a TWDP fading random variable in the numerator and the sum of TWDP fading random variables in the denominator. This probability distribution is in general not known in closed (or semi-closed) form [27]. Hence, it is difficult to guarantee a certain level of reliability of the multi-point transmissions.

2) Rate Adaptation and Outage Probability: Since the transmitter does not know the phase-shifts $\psi_{c,u}$ and $\psi_{c,u,j}$, transmission rate adaptation based on the instantaneous SINR is not possible. Instead, we consider a fixed-rate transmission with rate $\bar{r}_u(f_u)$ based on the mean macroscopic signal to noise ratio (SNR) of user u

$$\bar{r}_u(f_u) = \log_2\left(1 + f_u \bar{\beta}_u\right), \tag{16}$$

$$\bar{\beta}_u = \frac{\alpha_{1,u}^2 + \alpha_{2,u}^2 + 2\sigma_{h,u}^2}{2\sigma_n^2}. \tag{17}$$

Here, factor $0 < f_u \leq 1$ is introduced as a fading and interference penalty term to achieve a reliable transmission rate adaptation, as investigated in Section III-C.

Given rate $\bar{r}_u(f_u)$, the link is in outage whenever the instantaneous achievable rate $r_u = \log_2(1 + \beta_u)$ falls below $\bar{r}_u(f_u)$, or equivalently whenever $\beta_u < f_u \bar{\beta}_u$. Hence, the link outage probability is

$$p_{\text{out},u}(f_u) = \mathbb{P}\left(r_u < \bar{r}_u(f_u)\right) = \mathbb{P}\left(\beta_u < f_u \bar{\beta}_u\right). \tag{18}$$

Since we cannot calculate the probability distribution of the SINR β_u in the general case, we also cannot calculate the outage probability. Thus, if the goal is to guarantee a certain level of link reliability, it is necessary to reduce the SINR to a tractable case, such that we can calculate the outage probability. We pursue this approach in the following section.

III. RELIABLE MULTI-POINT TRANSMISSIONS

In this section, we propose methods to enhance the reliability of multi-point transmissions under TWDP fading conditions. We consider two aspects of reliability in our work: 1) the link outage probability and 2) the packet transmission success probability. The link outage probability gauges whether a successful transmission between transmitter and receiver at a given rate is possible at all or not; more specifically, it quantifies the probability that a communication link between transmitter and receiver cannot be established at a given rate. In Section III-A, we propose a zero-forcing based outage-optimized beamforming scheme for TWDP fading multi-point transmissions and, in

Section III-B, we propose a scheduling/link-grouping algorithm, which attempts to maximize the average transmission rate of the system under non-zero link outage probability. The packet success probability gauges the probability of successfully transmitting a packet of given size. Even for relatively high link outage probabilities, the packet success probability can be made large simply by retransmitting a packet multiple times, thereby exploiting diversity of the channel. However, this comes at the cost of consuming more resources (in time or frequency) for retransmissions. In Section III-C, we propose transmission rate adaptation methods to minimize the number of occupied resources for packet transmissions, assuming non-zero link outage probability as well as the utilization of hard-retransmission automatic repeat request (ARQ).

A. Beamforming Coordination

The instantaneous SINR in (15) is dictated by two fading effects: firstly, the multipath interference of the two dominant scatterers of each link due to random phases $\varphi_{c,u}$ and $\varphi_{c,u,j}$, and secondly, the power received over the diffuse channel components. Given the stated CSIT assumptions, i.e., unknown diffuse channel components $\mathbf{h}_{d,u}$ and $\mathbf{h}_{d,u,j}$, the transmitters cannot influence the second factor. However, the beamforming can be coordinated to control the amount of interference received over the interfering dominant scatterers.

1) Zero-Forcing of Dominant Interference: To obtain a tractable expression for the link outage probability, we propose to zero-force the interference over the dominant scattering clusters, by restricting the beamformer of link u to lie in the left null space of the dominant scattering clusters of the interference channels

$$\mathbf{f}_u \in \text{null}\left(\bar{\mathbf{H}}_u\right), \tag{19}$$

$$\bar{\mathbf{H}}_u = [\cdots, \mathbf{h}_{1,j,u}, \mathbf{h}_{2,j,u}, \cdots], j \in \mathcal{S}_g, j \neq u. \tag{20}$$

Matrix $\bar{\mathbf{H}}_u$ is of size $N_t \times 2(|\mathcal{S}_g| - 1)$. Thus, to obtain a non-empty left null space, the number of simultaneously active links is restricted by $S_g = |\mathcal{S}_g| \leq (N_t + 1)/2$. The factor 2 is because the transmitter does not know the relative phase-shift $\varphi_{1,j,u} - \varphi_{2,j,u}$ between the two dominant multipath components of each link. It is thus necessary to zero-force each of them individually.

We represent $\text{null}(\bar{\mathbf{H}}_u)$ by an orthogonal basis

$$\mathbf{B}_u \in \mathbb{C}^{N_t \times N_g}, \ N_g = N_t - 2(|\mathcal{S}_g| - 1), \tag{21}$$

$$\mathbf{B}_u^{\text{H}} \mathbf{B}_u = \mathbf{I}_{N_g}, \ \bar{\mathbf{H}}_u^{\text{H}} \mathbf{B}_u = \mathbf{0}. \tag{22}$$

This basis can, e.g., be obtained by applying a singular value decomposition (SVD) to $\bar{\mathbf{H}}_u$ and setting $\mathbf{B}_u$ equal to the left singular vectors corresponding to the zero-valued singular values. With this notation, we can write $\mathbf{f}_u = \mathbf{B}_u \mathbf{q}_u$, with $\mathbf{q}_u \in \mathbb{C}^{N_g \times 1}$ and $\|\mathbf{q}_u\| = P_u$. Thus, if $N_g > 1$, we still have a number of degrees of freedom left that can be utilized to optimize the intended link, as discussed below.

If all links adopt this zero-forcing approach, the interference between simultaneously active links is reduced to zero-mean statistically independent complex Gaussian terms of variance $2\sigma_{d,j,u}^2$, $j, u \in \mathcal{S}_g$, due to the diffuse channel components. These

interference terms cannot further be influenced by the choice of $\mathbf{q}_u$, since the transmitter does not know the diffuse channels $\mathbf{h}_{d,u,j}$.

2) Optimization of Intended Link: We next focus on the intended signal power of link u for the optimization of $\mathbf{q}_u$. The intended signal power is determined by the effective SISO channel

$$\bar{h}_u = \mathbf{h}_u^{\text{H}} \mathbf{B}_u \mathbf{q}_u = \left(\mathbf{B}_u^{\text{H}} \mathbf{h}_u\right)^{\text{H}} \mathbf{q}_u = \bar{\mathbf{h}}_u^{\text{H}} \mathbf{q}_u. \tag{23}$$

The absolute value $|\bar{h}_u|$ still follows TWDP fading statistics, however, with modified amplitudes

$$\bar{V}_{c,u} = \alpha_{c,u} \left|\bar{\mathbf{h}}_{c,u}^{\text{H}} \mathbf{q}_u\right|, \ \bar{\mathbf{h}}_{c,u} = \mathbf{B}_u^{\text{H}} \mathbf{h}_{c,u}, \ c \in \{1, 2\}, \tag{24}$$

$$\bar{z}_{d,u} = \bar{\mathbf{h}}_{d,u}^{\text{H}} \mathbf{q}_u \sim \mathcal{CN}\left(0, 2\bar{\sigma}_{d,u}^2\right), \ \bar{\mathbf{h}}_{d,u} = \mathbf{B}_u^{\text{H}} \mathbf{h}_{d,u}. \tag{25}$$

The power of the diffuse component is not changed, because $\mathbf{B}_u$ is semi-unitary; that is, $\bar{\sigma}_{d,u}^2 = \sigma_{d,u}^2$. We denote the fading parameters of this effective channel, as defined in (7) and (8), as $\bar{\Omega}_u$, $\bar{K}_u$ and $\bar{\Delta}_u$.

We have shown in [42] that the signal outage probability of a single-point TWDP fading link can be minimized by selecting the beamformer as

$$\mathbf{q}_u = \sqrt{P_u}\left(k_u \mathbf{q}_u^{\perp} + \sqrt{1 - k_u^2}e^{j\xi_u}\mathbf{q}_u^{\|}\right), \tag{26}$$

$$\mathbf{q}_u^{\perp} = \frac{\tilde{\mathbf{q}}_u^{\perp}}{\|\tilde{\mathbf{q}}_u^{\perp}\|}, \ \tilde{\mathbf{q}}_u^{\perp} = \left(\mathbf{I}_{N_g} - \frac{\bar{\mathbf{h}}_{2,u}\bar{\mathbf{h}}_{2,u}^{\text{H}}}{\|\bar{\mathbf{h}}_{2,u}\|^2}\right)\frac{\bar{\mathbf{h}}_{1,u}}{\|\bar{\mathbf{h}}_{1,u}\|}, \tag{27}$$

$$\mathbf{q}_u^{\|} = \frac{\bar{\mathbf{h}}_{2,u}}{\|\bar{\mathbf{h}}_{2,u}\|}, \ \xi_u = -\arg\left(\bar{\mathbf{h}}_{1,u}^{\text{H}}\bar{\mathbf{h}}_{2,u}\right), \ k_u \in [0, 1]. \tag{28}$$

Notice, this beamformer decomposition assumes that $\bar{V}_{1,u} \geq \bar{V}_{2,u}$; otherwise, the roles of $\bar{\mathbf{h}}_{1,u}$ and $\bar{\mathbf{h}}_{2,u}$ should be swapped. Scalar $k_u \in [0, 1]$ denotes a line-search parameter, which has to be optimized numerically to achieve minimal outage probability. Its optimal value depends on the fading parameters $\bar{\Omega}_u$, $\bar{K}_u$ and $\bar{\Delta}_u$ of the link, as well as, on the powers of noise and interference.

For $k_u = 1$, the beamformer is orthogonal to the weaker scatterer and aligns with the stronger scatterer in the orthogonal complement of $\bar{\mathbf{h}}_{2,u}$. In this case, fading of $|\bar{h}_u|$ is reduced to Rice fading, as there is effectively only one scattering cluster left; thus with $k_u = 1$ fading is minimized, however, at the cost of decreased average signal power. With $k_u < 1$, we can increase the average signal power, yet, then also the amount of fading grows, since both scattering clusters interfere. The optimal choice of k_u is therefore a trade-off between average signal power and amount of fading of the intended link.

Since the choice of $\mathbf{q}_u$ does not have an impact on the residual multi-point interference over the diffuse scattering channels, this beamformer decomposition is also outage-optimal for the considered multi-point transmission case, provided the line-search parameter k_u is properly chosen as discussed next.

Algorithm 1: Iterative Algorithm for the Calculation of the Outage Upper and Lower Bounds.

Input: Initial interval set $\mathcal{X}_0 = \left\{ \left[0, \sum_{j \in \mathcal{S}_g \setminus \{u\}} \sigma_{d,u,j}^2 \right), \left[\sum_{j \in \mathcal{S}_g \setminus \{u\}} \sigma_{d,u,j}^2, \infty \right) \right\}$ and desired level of accuracy $\epsilon > 1$.

Initialization: Interval number $N = 2$, loop counter $\ell = 0$.

Main:

1 **repeat**

2   Calculate the outage lower and upper bounds $p_{\text{out},u}^{(\text{lb})}(k_u, f_u)$, $p_{\text{out},u}^{(\text{ub})}(k_u, f_u)$ according to (33), (34) for interval set $\mathcal{X}_\ell$.

3   Find the interval $i^* : [x_{i^*}, x_{i^*+1}) \in \mathcal{X}_\ell$ for which the difference between upper and lower bound is largest:

$$i^* = \underset{i \in \{0, \dots, N-1\}}{\arg\max} \left(F_{|\bar{h}_u|} \left(\sqrt{f \bar{\beta}_u \left(\sigma_n^2 + x_{i+1} \right)} \right) - F_{|\bar{h}_u|} \left(\sqrt{f \bar{\beta}_u \left(\sigma_n^2 + x_i \right)} \right) \right) p_i.$$

     if $i^* < N - 1$ **then**

4   Split the interval i^* into two halves:

$$\mathcal{X}_{\ell+1} = \{ [x_0, x_1), \dots, [x_{i^*}, x_{i^*+1}/2), [x_{i^*+1}/2, x_{i^*+1}), \dots, [x_{N-1}, \infty) \}.$$

5   **else**

6   Split the last interval:

$$\mathcal{X}_{\ell+1} = \{ [x_0, x_1), \dots, [x_{N-1}, 2x_{N-1}), [2x_{N-1}, \infty) \}.$$

7   **end**

8   Update $N = N + 1$ and $\ell = \ell + 1$.

9 **until** $p_{out,u}^{(ub)}(k_u, f_u) / p_{out,u}^{(lb)}(k_u, f_u) < \epsilon$;

Output: Outage lower and upper bounds $p_{out,u}^{(\text{lb})}(k_u, f_u)$, $p_{out,u}^{(\text{ub})}(k_u, f_u)$.

---

3) Outage-Probability of Zero-Forcing Based Multi-Point Transmissions: With the choice of beamformer above, the instantaneous SINR of link u reduces to

$$\beta_u(k_u) = \frac{\left| \sum_{c=1}^2 \bar{V}_{c,u} e^{\mathrm{j}\bar{\psi}_{c,u}} + \bar{z}_{d,u} \right|^2}{2\sigma_n^2 + \sum_{j \in \mathcal{S}_g \setminus \{u\}} \left| \bar{z}_{d,u,j} \right|^2}. \tag{29}$$

This value is a function of the line-search parameter k_u, as it determines the amplitudes $\bar{V}_{c,u}$ of the effective TWDP link. However, it does not depend on the parameters k_j of the other links, because the effective interference terms are independent of k_j: $\bar{z}_{d,u,j} \sim \mathcal{CN}(0, 2\sigma_{d,u,j}^2)$.

The probability distribution of the instantaneous SINR (29) is determined by TWDP fading of the intended signal and by the probability distribution of the sum of Rayleigh fading interference terms. Let us consider the probability distribution of the instantaneous interference

$$I_u = \sum_{j \in \mathcal{S}_g \setminus \{u\}} |\bar{z}_{d,u,j}|^2 = \sum_{j \in \mathcal{S}_g \setminus \{u\}} I_{u,j}. \tag{30}$$

Since $\bar{z}_{d,u,j} \sim \mathcal{CN}(0, 2\sigma_{d,u,j}^2)$, each interference term $I_{u,j}$ follows a weighted chi-square distribution with two degrees of freedom, $|\bar{z}_{d,u,j}|^2 \sim \sigma_{d,u,j}^2 \cdot \chi_2^2$. The sum interference $I_u = \sum_{j \in \mathcal{S}_g \setminus \{u\}} I_{u,j}$ does generally not follow a weighted chi-square distribution, only in the special case that all variances $\sigma_{d,u,j}^2$ are equal, which is mostly not satisfied due to pathloss differences..[1] Nevertheless, the distribution of the sum interference, as a positively weighted sum of independent and identically distributed (iid) chi-square random variables, has been thoroughly studied in the literature and many efficient and accurate approximations

of its cdf are available [55]. Additionally, as we will see below, we only need to evaluate this cdf at few points to obtain virtually optimal performance. We denote the probability density function (pdf) and the cdf of the sum-interference I_u of user u as $f_{I_u}(x)$ and $F_{I_u}(x)$, respectively.

Rearranging terms inside probability (18) and utilizing the law of total probability, we write the outage probability of link u, as a function of the line-search parameter k_u, as

$$p_{\text{out},u}(k_u, f_u) = \int_0^\infty F_{|\bar{h}_u|} \left(\sqrt{f_u \bar{\beta}_u \left(2\sigma_n^2 + x \right)} \right) f_{I_u}(x) dx. \tag{31}$$

where $f_{I_u}(x)$ denotes the pdf of the sum of weighted chi-square interference terms $I_u = \sum_{j \in \mathcal{S}_g \setminus \{u\}} I_{u,j}$, and $F_{|\bar{h}_u|}(x)$ is the cdf of the TWDP fading random variable $|\bar{h}_u|$. The cdf of TWDP fading is given in integral-form in [29]. Thus, calculation of the outage probability of the proposed zero-forcing based multi-point beamforming scheme requires two-dimensional integration. To simplify this calculation, we propose below a simple bounding scheme.

4) Bounding of the Outage Probability: By splitting the integration interval $[0, \infty)$ of (31) into N contiguous intervals $\mathcal{X} = \{ [x_0 = 0, x_1), [x_1, x_2), \dots, [x_{N-1}, x_N = \infty) \}$ and by exploiting the monotonicity of the cdfs, we can immediately bound the outage probability as

$$p_{\text{out},u}^{(\text{lb})}(k_u, f_u) \leq p_{\text{out},u}(k_u, f_u) \leq p_{\text{out},u}^{(\text{ub})}(k_u, f_u), \tag{32}$$

$$p_{\text{out},u}^{(\text{lb})}(k_u, f_u) = \sum_{i=0}^{N-1} F_{|\bar{h}_u|} \left(\sqrt{f_u \bar{\beta}_u \left(2\sigma_n^2 + x_i \right)} \right) p_i, \tag{33}$$

$$p_{\text{out},u}^{(\text{ub})}(k_u, f_u) = \sum_{i=0}^{N-1} F_{|\bar{h}_u|} \left(\sqrt{f_u \bar{\beta}_u \left(2\sigma_n^2 + x_{i+1} \right)} \right) p_i, \tag{34}$$

---

[1]Equal pathloss would be reasonable in a point to multi-point multi-user MIMO situation, where all links are with respect to the same transmitter; however, in this case the interference channels would be correlated and not statistically independent, which further complicates the analysis [27]

Algorithm 2: Greedy Link Scheduling Coordination Algorithm based on Mutual Channel Coherence.

Input: Channels of scattering clusters $\mathbf{h}_{c,i,j}$, $\forall c \in \{1, 2\}$, $\forall i, j \in \{1, \ldots, N_u\}$.

Initialization:

Maximal group size according to zero-forcing dimensionality constraint $N_{\max} = \lfloor (N_t + 1)/2 \rfloor$.

Minimal number of scheduling groups $N_{s,\min} = \lceil N_u/N_{\max} \rceil$.

Mutual coherence of intended and interfering links:

$$\rho_{i,j} = \left\| \left(\mathbf{H}_i \left(\mathbf{H}_i^{\mathrm{H}} \mathbf{H}_i \right)^{-1} \mathbf{H}_i^{\mathrm{H}} \right) \left(\mathbf{H}_{i,j} \left(\mathbf{H}_{i,j}^{\mathrm{H}} \mathbf{H}_{i,j} \right)^{-1} \mathbf{H}_{i,j}^{\mathrm{H}} \right) \right\|,$$

$\mathbf{H}_i = [\mathbf{h}_{1,i}, \mathbf{h}_{2,i}]$, $\mathbf{H}_{i,j} = [\mathbf{h}_{1,i,j}, \mathbf{h}_{2,i,j}]$, $\forall i, j \in \{1, \ldots, N_u\}, j \neq i$.

Ordered list of link indices $\mathcal{N}_u = \{\ldots, m, n, \ldots\}$ sorted according to decreasing maximal mutual coherence:

$$\rho_{m,\max} = \max_j \rho_{m,j} \geq \rho_{n,\max} = \max_j \rho_{n,j}, \; m, n \in \{1, \ldots, N_u\}.$$

Main:

1 **for** $N_s \in \{N_{s,min}, \ldots, N_u\}$ **do**

2   Determine valid group sizes $\lfloor N_u/N_s \rfloor \leq S_\ell \leq \lceil N_u/N_s \rceil$, $\ell \in \{1, \ldots, N_s\}$, such that, $\sum_{\ell=1}^{N_s} S_\ell = N_u$.

3   Initialize scheduling groups $\mathcal{S}_\ell = \mathcal{N}_u(\ell)$, $\ell \in \{1, \ldots, N_s\}$ to split-off the links with largest mutual coherence.

4   **for** $\ell \in \{1, \ldots, N_s\}$ **do**

5   **for** $k \in \{2, \ldots, S_\ell\}$ **do**

6   Find the link with minimal mutual coherence to the already scheduled links of group ℓ:

$$j^* = \arg \min_j \sum_{i \in \mathcal{S}_\ell} \frac{1}{2} \left(\rho_{i,j} + \rho_{j,i} \right), \; j \in \{1, \ldots, N_u\} \setminus \cup_{n=1}^{N_s} \mathcal{S}_n$$

             Add link j^* to the scheduling group: $\mathcal{S}_\ell = \mathcal{S}_\ell \cup j^*$.

7   **end**

8   Determine the outage probabilities $p_{\mathrm{out},u}$ of all links in group $\mathcal{S}_\ell$ (utilizing outage optimal beamformers according to Sec. III-A or any other beamformers).

9   **end**

10   Calculate the average rate $\bar{R}_{N_s}$ for N_s scheduling groups according to (37).

11 **end**

12 Find the optimal number of scheduling groups:

$$N_s^* = \arg \max_{N_s \in \{N_{s,\min}, \ldots, N_u\}} \bar{R}_{N_s}.$$

Output: Optimized scheduling groups $\mathcal{S}_\ell^*$, $\ell \in \{1, \ldots, N_s^*\}$.

$$p_i = F_{I_u}(x_{i+1}) - F_{I_u}(x_i). \tag{35}$$

The accuracy of the bounds is determined by the interval set $\mathcal{X}$. This set can efficiently be discovered iteratively to achieve a desired level of accuracy $p_{\mathrm{out},u}^{(\mathrm{ub})}(k_u, f_u)/p_{\mathrm{out},u}^{(\mathrm{lb})}(k_u, f_u) < \epsilon$, $\epsilon > 1$, as described in Algorithm 1. This simplifies the outage calculation to one-dimensional integration for the evaluation of the TWDP fading cdf.

5) Outage-Based Parameter Optimization: Utilizing Algorithm 1, we can now proceed to optimize the parameter k_u

$$k_u^*(f_u) = \arg \min_{k_u \in [0,1]} \frac{p_{\mathrm{out},u}^{(\mathrm{ub})}(k_u, f_u) + p_{\mathrm{out},u}^{(\mathrm{lb})}(k_u, f_u)}{2}. \tag{36}$$

This can be achieved by applying a line-search algorithm on the interval $k_u \in [0, 1]$, e.g., the bisection method [56], or by sampling the interval with a satisfactory resolution. We denote the corresponding outage probability as $p_{\mathrm{out},u}^*(f_u) = p_{\mathrm{out},u}(k_u^*(f_u), f_u)$.

Analyzing the complexity of Algorithm 1 is not straightforward, as the number of iterations of the loop depends on the desired level of accuracy ϵ and we have unfortunately neither been able to find an analytic expression nor an upper bound for this number. Nevertheless, we can analyze the complexity of

an individual run of the loop to provide a hint on complexity. Within the loop, the cdf of N TWDP fading random variables has to be evaluated. In general, this requires numeric integration; however, we expect that in practice this would be realized in low complexity by a table look-up instead, employing a precomputed table for a range of values of the cdf. Additionally, the values p_i of Eq. (35) must be calculated, by evaluating the cdf expression of [55]; again, in practice this could be realized by a table look-up. Thus, within each loop iteration, at most work of complexity $O(NT)$ has to be performed, if the look-ups in the tables of size T are realized by (inefficient) brute force search. As we show in our simulations in Section IV-A, for the optimization of the line-search parameter k_u in (36) a small number of expansion terms/intervals N (in the order of two to four) is sufficient to achieve virtually optimal performance; hence, the complexity of beamformer optimization is still manageable. To reduce the level of accuracy of the outage upper and lower bounds down to $\epsilon \approx 1.25$ around ten to fifteen expansion terms are necessary in our simulations.

B. Scheduling Coordination

The performance of the beamforming coordination approach described above strongly depends on the set of links that operate concurrently and thus interfere with the intended link. Therefore, by coordinating the set of links that are simultaneously active

we can influence the link outage probability and, e.g., maximize the average rate of the system

$$\bar{R}_{N_s} = \frac{1}{N_s} \sum_{\ell=1}^{N_s} R_\ell = \frac{1}{N_s} \sum_{\ell=1}^{N_s} \sum_{u \in \mathcal{S}_\ell} \left(1 - p_{\text{out},u}(f_u) \right) \bar{r}_u(f_u), \tag{37}$$

where R_ℓ denotes the rate of scheduling group ℓ.

Unfortunately, such an optimization is not possible in closed-form. It rather requires an exhaustive search over all possible set partitions of set $\{1, \ldots, N_u\}$. The number of set partitions grows exponentially with N_u according to the well studied Bell numbers [57]. This optimization thus becomes infeasible very quickly with growing N_u.

We therefore resort to greedy link scheduling coordination as summarized in Algorithm 2. The rationales behind this algorithm are:

- The main scheduling metric for link grouping is the mutual coherence $\rho_{i,j}$ of the channels of different links as defined in Algorithm 2. This mutual coherence gauges the overlap of the subspace spanned by the intended channel $\mathbf{H}_i = [\mathbf{h}_{1,i}, \mathbf{h}_{2,i}]$ with the subspaces spanned by the interfering channels $\mathbf{H}_{i,j} = [\mathbf{h}_{1,i,j}, \mathbf{h}_{2,i,j}]$. It therefore strongly impacts the zero-forcing solution (19). In line 6 of Algorithm 2, we attempt to determine scheduling groups $\mathcal{S}_\ell$ with minimal mutual coherence.
- We only consider set partitions where the sizes of the individual subsets are (approximately) equal $|\mathcal{S}_i| \approx |\mathcal{S}_j|, \forall i, j \in \{1, \ldots N_s\}$. Exact equality is only feasible if N_u/N_s is integer; otherwise, some sets are of size $\lceil N_u/N_s \rceil$ and others of size $\lfloor N_u/N_s \rfloor$, such that each link is part of exactly one group. This is reasonable, since we schedule different groups in a round-robin fashion at different time instances. Thus, if there was a strong imbalance in the group size, the groups with a small number of links would achieve high rates, whereas the others would suffer from low rates, leading to an unfair resource allocation.
- We test all feasible group numbers $N_s \in \{N_{s,\text{min}}, \ldots, N_u\}$, where $N_{s,\text{min}}$ is the minimum number of groups necessary to satisfy the zero-forcing dimensionality constraint $|\mathcal{S}_g| \leq (N_t + 1)/2, \quad \forall g \in \{1, \ldots N_s\}$. The optimal group number N_s^*, which maximizes the average rate $\bar{R}_{N_s}$, is basically a trade-off between the achieved link outage probability and the scheduling time interval of the groups. Smaller group sizes (larger N_s) achieve lower link outage probabilities; however, with a growing number N_s of groups, the round-robin scheduling time interval increases, implying that each group is scheduled less frequently in time.

This algorithm contains three relatively complex tasks. 1) Calculating the mutual coherence values $\rho_{i,j}$: These values have to be calculated for all pairs (i, j) with $i \neq j$, i.e., $N_u(N_u - 1)$ values. Each value requires two inversions of matrices of size 2×2 and six multiplications of matrices with larger dimension equal to N_t. This therefore has a total complexity order of $O(N_u^2 N_t^3)$. 2) Running through three nested for-loops to determine the schedule: The size of the outer for-loop is at most N_u

and that of the two inner for-loops together is also N_u. Additionally, within the innermost loop a search over at most N_u values has to be performed. The total complexity is therefore in the order $O(N_u^3)$. 3) Calculating the outage probabilities of all links within the center loop of the scheduling algorithm: This has a total complexity order $O(N_u^2 O(\text{Alg1}))$, with $O(\text{Alg1})$ denoting the complexity of Algorithm 1. For very large numbers of users, the complexity of the scheduling algorithm become intractable. However, in practice it is only necessary to coordinate links that are in close spatial proximity, which should help keeping the complexity manageable.

C. Transmission Rate Adaptation

In this section, we discuss the selection of the user rate $\bar{r}_u(f_u)$ via the fading penalty parameter $0 < f_u \leq 1$. There are a number of reasonable possibilities for selecting f_u:

- If the schedule of the links $\mathcal{S}_\ell, \forall \ell \in \{1, \ldots, N_s\}$ is fixed, one viable approach for selecting f_u is to achieve a target outage probability. In combination with the beamforming coordination of Section III-A, this requires a line search over f_u in which $p_{\text{out},u}^*(f_u)$ is iteratively updated.
- If the link schedule is not fixed, we can consider the same fading penalty $f_u = f$ for all links, in order to jointly optimize it with the scheduling coordination of Section III-B. The fading penalty impacts the average system rate of a given link schedule according to (37) via the average rate $\bar{r}_u(f_u)$ (16). Hence, our greedy scheduling Algorithm 2 can be combined with a line search over f to maximize the average system rate.

The methods described above for selection of the fading penalty f_u are suitable for full data buffer transmissions. Below, however, we focus on transmissions of packets of fixed size of P bits (e.g., cooperative awareness messages in the context of V2X). We assume that the TWDP fading of the channel is approximately constant over a duration of T_c seconds (coherence time) and a bandwidth of B_c Hertz (coherence bandwidth). We denote the product $T_c B_c$ as a coherence block (CB). We adopt a block-fading channel model where the TWDP fading channel realizations of different CBs are uncorrelated, yet with the same macroscopic channel parameters; i.e., only the phases $\varphi_{c,u}, \varphi_{c,u,j}$ and the diffuse channel components vary randomly in-between CBs.

During one CB, the number of transmitted bits is

$$P_u(f_u) = B_c T_c \log_2 \left(1 + f_u \bar{\beta}_u \right), \tag{38}$$

provided the transmission is successful; otherwise, it is zero. Thus, the minimal number of required successful CBs to transmit a single packet is $L_u^{\text{min}}(f_u) = \lceil P/P_u(f_u) \rceil$. We assume that transmission errors during a CB can be detected by the receiver, e.g., by a cyclic redundancy check (CRC). In case of a transmission error, an ARQ retransmission of the data of the respective coherence block is initiated.

The goal of our proposed transmission rate selection method is to minimize the required number $L_u(f_u)$ of CBs (including possible retransmissions) for successful transmission of a complete packet of P bits. Since our system operates at non-zero

link outage probability, we cannot impose a hard constraint on this number. Instead, we select the fading penalty f_u such as to minimize an upper bound $L_{\max}$ on the required number of CBs, which is violated with low probability $p_{\max}$

$$\min_{0 < f_u \leq 1} L_{\max},$$

$$\text{s.t. } p_u(f_u, L_{\max}) = \mathbb{P}\left(L_u(f_u) > L_{\max}\right) \leq p_{\max}. \quad (39)$$

Here, $p_u(f_u, L_{\max})$ denotes the probability that more than $L_{\max}$ CBs are required for the transmission of a packet.

The probability that the required number $L_u(f_u)$ of CBs is larger than $L_{\max}$, as a function of f_u, can be written as

$$p_u(f_u, L_{\max}) = \dots$$

$$\begin{cases} 1 - \mathbb{P}\left(L_u(f_u) \leq L_{\max}\right), & L_{\max} \geq L_u^{\min}(f_u) \\ 1, & L_{\max} < L_u^{\min}(f_u) \end{cases}. \quad (40)$$

That is, we require at least $L_u^{\min}(f_u)$ successful CBs. Given $L_{\max} \geq L_u^{\min}(f_u)$, $p_u(f_u, L_{\max})$ is equal to one minus the packet success probability.

Let us consider the non-trivial case $L_{\max} \geq L_u^{\min}(f_u)$, i.e., $L_{\max} = L_u^{\min}(f_u) + \Delta L_{\max}$, $\Delta L_{\max} \geq 0$. In this case, we can develop the packet success probability as

$$\mathbb{P}\left(L_u(f_u) \leq L_{\max}\right) = \sum_{t=0}^{\Delta L_{\max}} \mathbb{P}\left(L_u(f_u) = L_u^{\min}(f_u) + t\right), \quad (41)$$

$$\mathbb{P}\left(L_u(f_u) = L_u^{\min}(f_u) + t\right) = \binom{L_u^{\min}(f_u) + t - 1}{L_u^{\min}(f_u) - 1} \dots$$

$$\left(p_{\text{out},u}(f_u)\right)^t \left(1 - p_{\text{out},u}(f_u)\right)^{L_u^{\min}(f_u)}, \quad (42)$$

with $p_{\text{out},u}(f_u)$ as defined in (18) or (31) for our proposed beamforming scheme. Here, the second equality follows from a simple combinatorial argument: during the first $L_u^{\min}(f_u) + t - 1$ CBs exactly $L_u^{\min}(f_u) - 1$ arbitrarily positioned transmission are successful and t transmissions fail, whereas the transmission in CB $L_u^{\min}(f_u) + t$ has to be correct to achieve $L_u(f_u) = L_u^{\min}(f_u) + t$. We observe that this probability is governed by two competing effects: on the one hand, by increasing f_u the minimal number of required successful CB transmissions $L_u^{\min}(f_u)$ can be reduced; on the other hand, increasing f_u also causes an increase in the outage probability $p_{\text{out},u}(f_u)$ of each CB transmission and thus requires more retransmissions. Therefore, an optimal choice of f_u exists, which balances these two effects.

Notice, in case that CBs are only assigned in the time domain, $L_u(f_u)$ is equivalent to the transmission latency of the user in terms of the number of coherence times T_c.

IV. SIMULATIONS

In this section, we investigate the performance of the proposed techniques by numerical link level simulations. For all simulations, we generate one hundred iid random realizations of the channels $\mathbf{h}_{c,u,j}$ (sum over all rays within cluster c) according to $\mathbf{h}_{c,u,j} \sim \mathcal{CN}(\mathbf{0}, 1/N_t\,\mathbf{I})$, assuming that each cluster is

composed of many rays. For each random realization of the channels of the scattering clusters $\mathbf{h}_{c,u,j}$ we numerically determine the link outage probability by generating ten thousand iid random realizations of the diffuse channels and the phases of the two scattering clusters. We consider iid channel realizations for the microscopic fading, since the channel in the mmWave band varies significantly even for small movement of the users due to the short millimeter-scale wavelength.

We assume that the two scattering clusters are equally strong $\alpha_{1,u,j} = \alpha_{2,u,j}$. This corresponds to a worst case in terms of TWDP outage behavior, because it leads to very deep fades whenever the signals received over these two clusters add up destructively. We consider a ratio of dominant scattering power to diffuse power of $(\alpha_{1,u,j}^2 + \alpha_{2,u,j}^2)/(2\sigma_{h,u,j}^2) = 100$. This choice is motivated by our observations from V2X channel measurements [47], where TWDP K-factors in the order of 20 to 30 dB have been measured. We normalize the average power of the intended channel as $\alpha_{1,u}^2 + \alpha_{2,u}^2 + 2\sigma_{h,u}^2 = 1$ and set the noise variance equal to $2\sigma_n^2 = 0.01$; thus, the mean macroscopic SNR of each user is $\bar{\beta}_u = 20$ dB. We consider a relatively high SNR, since we want to emphasize outage effects caused by mutual interference. We assume that all interfering channels are weaker by a factor γ than the intended channel; we specify the considered value of γ below. We simulate scenarios with relatively strong interference for uncoordinated transmissions (cell-edge scenarios); this is to highlight the gains achievable by coordinating inter-cell interference. Finally, we consider unit transmit power $P_u = 1$ for all links.

A. Beamforming Approaches

In our first simulations, we investigate the beamforming coordination of Section III-A. We first consider a scenario with $N_t = 16$ transmit antennas and $N_u = 6$ links, which are all active simultaneously; that is, there is just one scheduling group in which all links are co-scheduled and thus $S_g = |\mathcal{S}_g| = N_u$. We assume that all interfering channels are weaker by a factor $\gamma = \frac{1}{N_u - 1}$ than the intended channel, such that the average sum power of the interfering channels is equal to the average power of the intended channel. In Fig. 2, we show the outage probability $p_{\text{out},u}(f_u)$ averaged over all links as a function of the fading penalty $f_u = f, \forall u \in \{1, \dots, N_u\}$. We compare the empirical outage probability (the two curves with markers) to the outage upper and lower bounds (33), (34), using $N \in \{2, 4, 12\}$ expansion terms. We observe that the gap between the upper and lower bounds diminishes quickly with growing number of expansion terms. For $N = 12$ expansion terms, the accuracy level ϵ of Algorithm 1, i.e., the ratio of outage upper and lower bounds, is already reduced to $\epsilon \approx 1.25$. The two empirical outage curves have been obtained with beamformers that have been optimized according to (36), utilizing $N \in \{2, 12\}$ expansion terms for the outage bounds. We observe that the performance in both cases is very similar, even though the outage upper and lower bounds for $N = 2$ exhibit a large gap. A small number of $N = 2$ to 4 expansion terms is therefore sufficient for the optimization of the beamformer, which supports an implementation with reduced complexity.
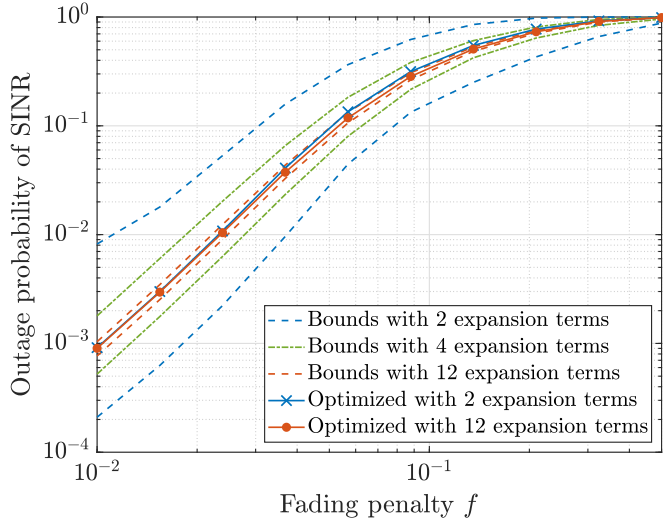
Fig. 2. Comparison of analytic outage bounds (33), (34) to empirical results, considering $N_t = 16$ transmit antennas and $N_u = 6$ active links.
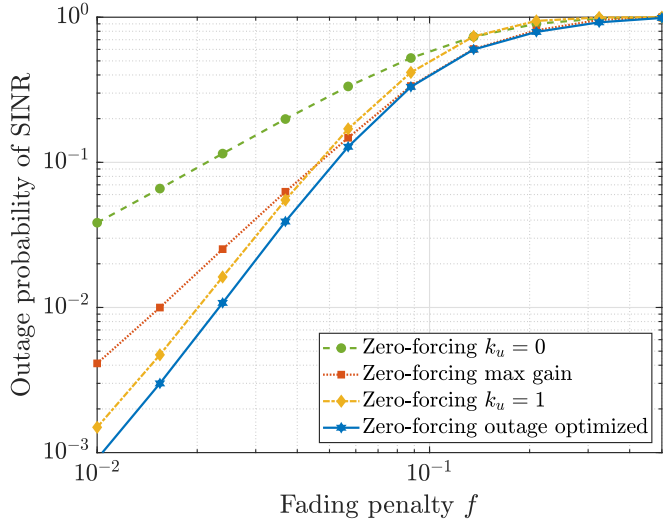

Fig. 3. Comparison of zero-forcing based beamforming schemes.

We next investigate the impact of the line-search parameter k_u, cf. (26), on the outage performance of the system. We consider $k_u \in \{0, 1\}$, our outage-optimized choice $k_u^*(f_u)$ of (36) and zero-forcing max gain beamforming according to (44). The results are shown in Fig. 3. As expected, the outage-optimized design achieves the lowest link outage probability. However, the gap to the solution with $k_u = 1$ is relatively small, especially for small values of $N_u = S_g$. This is because in this case the dimension $N_g = N_t - 2(S_g - 1)$ of the null space null($\bar{\mathbf{H}}_u$) is relatively large, such that we do not lose to much intended signal power if we align vector $\mathbf{q}_u$ with $\mathbf{q}_u^\perp$ in (26). Notice that the solution with $k_u = 1$ minimizes the amount of fading of the intended signal power, as the transmission is orthogonal to the weaker scattering cluster. Thus, this solution reduces the effective channel to Rice-fading rather than TWDP fading. For large transmissions rates, i.e., large values of the fading penalty f_u, zero-forcing max gain achieves the same performance as the outage-optimal choice of k_u, showing that in this regime it is most important to achieve a large signal power gain.

In our next simulation, we consider $N_t = 12$ and vary the number of simultaneously active links $N_u \in \{3, 4, 5\}$. We compare our outage optimized beamformer of Section III-A to the benchmark schemes described in Appendix A. In Fig. 4, we compare the performance of these beamforming schemes for various numbers of active links. We observe that the interference-agnostic max gain beamformer performs worse than the outage optimized zero-forcing solution. That is, for a given outage probability, the zero-forcing outage optimized solution supports a larger fading penalty and therefore a higher transmission rate than max gain beamforming; however, this gap reduces with growing N_u. This is because the zero-forcing solution increasingly causes a loss of intended signal power with decreasing null space dimension N_g. Therefore, the outage probability of the zero-forcing solution degrades with growing N_u. For $N_u = 6$ (not shown in the figure), which is the maximum possible number of links for zero-forcing, the max gain solution would already outperform the zero-forcing solution. The robust max-min SINR beamforming solution, as derived in Appendix A, performs similar to max gain beamforming, with slight gains at small values of the fading penalty. The approach based on the signal to leakage and noise ratio (SLNR) requires a very conservative selection of the transmission rate to achieve small outage probabilities; it is therefore not well suited for efficient multi-user transmissions with high reliability. Notice that we can analytically calculate the outage probability only for zero-forcing based beamforming, as the distribution of the SINR is not known for the other approaches. This implies that we can analytically guarantee a certain link reliability only under zero-forcing.

Since the solution with $k_u = 1$ performs close to optimal for smaller values N_u compared to N_t, we employ only this scheme in our remaining simulations. Notice, that this simplifies the outage calculations a lot, as we can then utilize the closed-form cdf of Rice-fading in (31) rather than the integral expression of TWDP fading.

B. Scheduling Coordination

We next investigate the proposed scheduling algorithm of Section III-B. For these simulations, we consider $N_t = 32$ transmit antennas and utilize our zero-forcing beamforming of Section III-A with $k_u = 1$. We assume that all interfering channels are weaker by a factor $\gamma = 0.5$ than the intended channel, corresponding to a relatively strong interference situation. We consider a total number of $N_u \in \{2, 3, 4, 6, 8, 10\}$ links and investigate the average rate performance according to (37) as a function of the fading penalty $f_u = f$, $\forall u$. Our scheduling coordination splits the total number N_u of links into subsets of active links according to Algorithm 2. These subsets are scheduled in a round robin fashion at different time instances to reduce the amount of interference; thus, if a total of N_s scheduling groups is formed, each group is only served on a fraction $1/N_s$ of the time/frequency resources.

In Fig. 5, we show the average rate $\bar{R}_{N_s}$ versus the fading penalty for different numbers of links N_u. Let us consider the curve for $N_u = 10$ to explain the observed behavior, as it most distinctly features two peaks: Initially, for small values of the
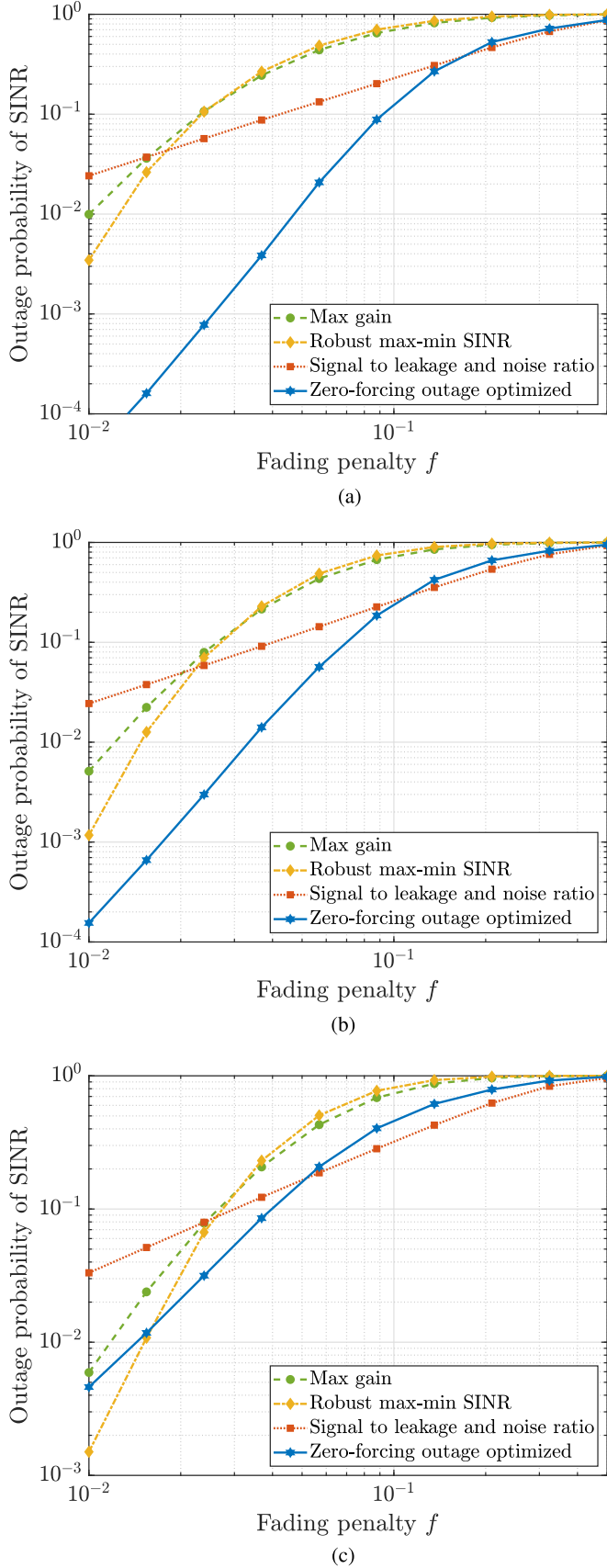
(a)

(b)

(c)

Fig. 4. Comparison of different beamforming schemes for $N_t = 12$ transmit antennas and $N_u \in \{3, 4, 5\}$ active links.
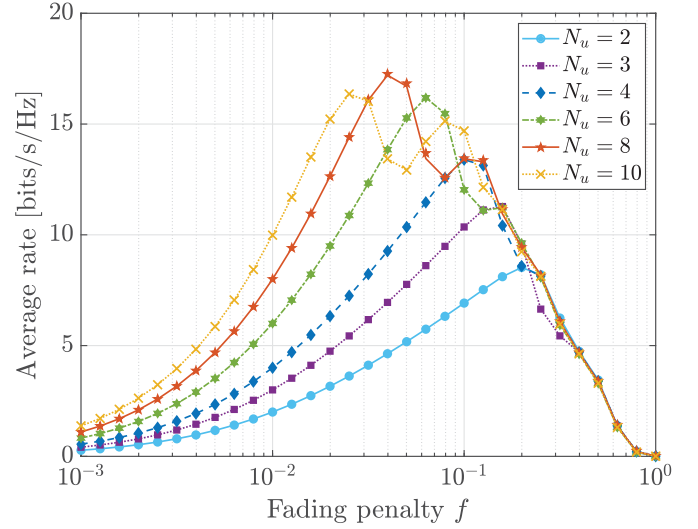

Fig. 5. Average rate versus fading penalty achieved by the proposed scheduling coordination algorithm for different numbers of links N_u.

fading penalty ($f_u = f <= 0.025$), all $N_u = 10$ links are simultaneously scheduled, i.e., $N_s = 1$ and $\mathcal{S} = \{1, \dots, N_u\}$, and the link outage probability $p_{out,u}(f_u)$ is very low for each link. With increasing fading penalty $f_u = f$, the links transmit with a higher rate $\bar{r}_u(f_u)$ and therefore the average rate of the system goes up according to (37). However, as we can see in (37), the average rate is not only determined by the transmit rate $\bar{r}_u(f_u)$, but also by the link outage probability $p_{out,u}(f_u)$: when we increase f_u, the term $\bar{r}_u(f_u)$ increases, but simultaneously the term $(1 - p_{out,u}(f_u))$ decreases. At the first peak at $f_u = 0.025$, these two effects balance each other for the case $N_s = 1$. With further increasing f_u, the term $(1 - p_{out,u}(f_u))$ becomes dominant and the average rate $\bar{R}_{N_s}$ starts to go down. However, at this point it still does not pay-off to split the total set of $N_u = 10$ links into two scheduling groups, which would then be multiplexed in time, since each group could then only transmit half of the time, causing a larger rate loss than caused by link outages. Yet, when we further increase f_u, at approximately $f_u = 0.05$, the outage probability $p_{out,u}(f_u)$ becomes so large, that it is better to split the schedule up into $N_s = 2$ groups, each consisting of only five users $S_1 = S_2 = 5$. By this, the outage probability of each group is reduced and the rate again starts to increase with growing $f_u = f$. From here on, the same argumentation starts to repeat: the increase of the average rate due to growing $\bar{r}_u(f_u)$ and its reduction due to decreasing $(1 - p_{out,u}(f_u))$ balance each other at $f_u = 0.08$ for the case $N_s = 2$ and afterwards the rate starts to deteriorate again. With further increasing f_u further splits of the schedule occur, however, they do not lead to pronounced peaks in the rate any more, as the outage probability cannot be sufficiently reduced by further splitting the schedule.

In our simulation, the best performance is achieved for $N_u = 8$ simultaneously active links when $f \approx 0.04$. Notice that the case $N_u = 10$ cannot achieve this performance for the following reason: In principle, the scheduler could decide to split the $N_u = 10$ users into two groups, one of size $S_1 = 8$ and one of size $S_2 = 2$. Then the group with $S_1 = 8$ active links would
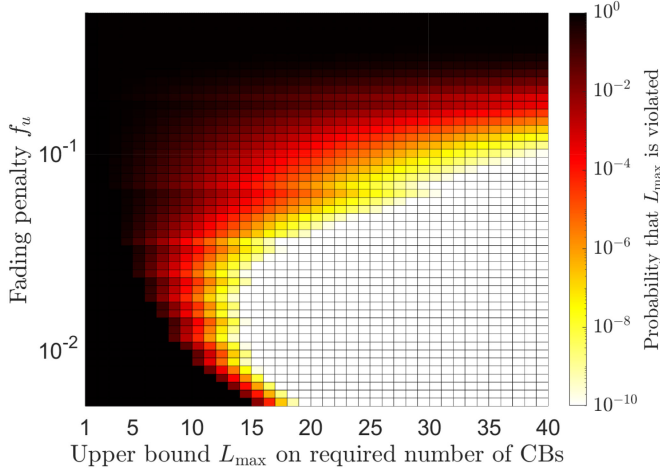
Fig. 6. Probability that the required number $L_u(f_u)$ of CBs is larger than $L_{\max}$ according to (40), as a function of the fading penalty f_u, for $N_t = 16$ transmit antennas and $N_u = 6$ simultaneously active links with outage optimized beamforming.

Fig. 7. Average number of required CBs of different beamforming schemes with optimized fading penalty f_u as a function of the number of transmit antennas.

achieve the same performance as the case $N_u = 8$ shown in the figure. However, the group with $S_2 = 2$ users would achieve the same performance as the case $N_u = 2$ and time-sharing between these two subsets would perform much worse than the fifty-fifty split ($S_1 = S_2 = 5$) performed by our optimized scheduling algorithm.

Notice, even though not shown in the figure, we also simulated an exhaustive search over all possible link partitions for up to $N_u = 6$, corresponding to 203 possible link schedules. Up to this number, we did not observe a noticeable difference between our proposed greedy scheduler and the exhaustive search. We could, however, not simulate the exhaustive search for $N_u \in \{8, 10\}$ for complexity reasons, as the number of possible link partitions becomes too large, namely $\{4140, 115\,975\}$.

C. Transmission Rate Selection

In this section, we investigate the number of required CBs for successful packet transmission, utilizing the optimized transmission rate selection of Section III-C. We consider $N_t = 16$ transmit antennas and a single scheduling group of $N_u = 6$ simultaneously active links. We employ a packet size of $P = 1.25 B_c T_c \log_2(1 + \bar{\beta}_u)$; that is, for a fading penalty of $f_u = 1$, $N_p(1) = \lceil 1.25 \rceil = 2$ error free CBs are required to transmit a single packet.

In our first simulation, we evaluate the probability that the required number $L_u(f_u)$ of CBs is larger than $L_{\max}$ according to (40) as a function of the fading penalty f_u, utilizing our outage optimized beamformer of Section III-A. The results are shown in Fig. 6. We observe that the performance is very poor for large values of f_u, simply because the SINR outage probability $p_{\text{out},u}(f_u)$ of the link is too high and therefore many retransmissions are required. For very low values of f_u, the performance is also not good, because the number $L_u^{\min}(f_u)$ of required error free CBs is too large. The sweet-spot for our simulation scenario lies at $f_u \approx 0.015$, where the SINR outage probability is relatively low and $L_u^{\min}(f_u)$ is also not excessively large.
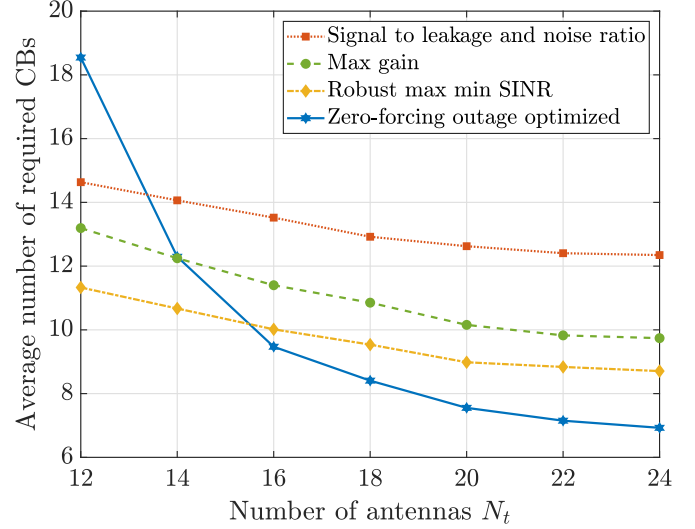
We next investigate the average number of required CBs for a maximal bound violation probability $p_{\max} = 10^{-5}$, as a function of the number of transmit antennas $N_t \in [12, 24]$ and $N_u = 6$ simultaneously active links. Notice, this bound violation probability corresponds to a packet transmission success probability of $99.99\,999\,\%$. The results are shown in Fig. 7 comparing the same beamforming schemes as in Section IV-A. We observe that the zero-forcing solution does not exhibit good performance if the number of antennas is too small; that is, the zero-forcing solution requires at least a certain minimum number of excess degrees of freedom ($N_g > 6$ in our example) to be able to cancel the multi-point interference and at the same time achieve sufficiently large signal power for the intended signal. However, with $N_t > 16$ and therefore $N_g > 16 - 2(6 - 1) = 6$ the zero-forcing solution achieves the required packet success probability with the smallest number of CBs compared to the other schemes.

V. CONCLUSION

Reliable communication architectures have to be able to accurately predict the outage performance of the offered service. In wireless communications, this is often hard as the probability distribution of the SINR of the communication link can in many cases not be characterized analytically. In this paper, we have proposed a coordinated beamforming scheme for directional MISO TWDP V2I fading channels, which allows such an analytic characterization under relatively mild CSIT assumptions. Based on this characterization, we have developed scheduling and rate adaptation techniques that facilitate reliable wireless transmissions, i.e., transmissions with guaranteed outage performance, and we have demonstrated the performance of these techniques by numerical experiments.

The presented framework can in principle be extended to more than two dominant scattering clusters. However, an analytic characterization of the fading distribution of the effective channel becomes more and more difficult with growing number

of specular components [58] and the proposed zero-forcing solution becomes increasingly inefficient, as it costs too many degrees of freedom to cancel the dominant interference. Nevertheless, as TWDP fading is known to represent a worst-case in terms of outage behavior, it is a sensible assumption for a reliable system design.

APPENDIX
BENCHMARK SCHEMES

We utilize the following beamforming schemes as benchmarks in our numerical simulations. Notice, only for the zero-forcing based schemes is it possible to analytically calculate the outage probability of the transmissions according to Section III-A3; hence, only these schemes can guarantee a desired level of reliability.

a) Max gain beamforming. The max gain beamformer aligns the beamforming vector $\mathbf{f}_u$ of user u with the stronger scattering cluster

$$\mathbf{f}_u = \sqrt{P_u} \frac{\mathbf{h}_{c_{\max},u}}{\|\mathbf{h}_{c_{\max},u}\|}, \ c_{\max} = \max_{c \in \{1,2\}} \alpha_{c,u} \|\mathbf{h}_{c,u}\|. \tag{43}$$

This beamforming vector does not account for the multi-point interference, which can lead to high outage probability.

b) Zero-forcing with fixed line-search parameter. The zero-forcing beamforming vectors with fixed line-search parameter k_u cancel the multi-point interference over the scattering clusters according to (19), but do not optimize the line-search parameter k_u in (26). In our simulations, we consider the two extreme cases $k_u \in \{0, 1\}$, to show how strongly the line-search parameter can impact the outage performance.

The case $k_u = 1$ reduces the effective channel to Rice fading, since the beamforming vector is orthogonal to the weaker scattering cluster. Thereby, fading of the effective channel (23) is minimized; however, the average signal power also be small. Conversely, for $k_u = 0$, the beamforming vector is aligned with the weaker scattering cluster, which can provide a gain in terms of average signal power, however, for the cost of increased channel fading, due to multipath interference of the two scattering clusters.

c) Zero-forcing max gain beamforming. The zero-forcing max gain beamforming vector applies interference cancellation according to (19) and aligns vector $\mathbf{q}_u$ with the stronger scattering cluster after projection onto the null space $\text{null}(\bar{\mathbf{H}}_u)$. The corresponding solution for k_u can be determined in closed-form

$$k_u = \left\| \left(\mathbf{I}_{N_g} - \frac{\bar{\mathbf{h}}_{2,u} \bar{\mathbf{h}}_{2,u}^H}{\|\bar{\mathbf{h}}_{2,u}\|^2} \right) \frac{\bar{\mathbf{h}}_{1,u}}{\|\bar{\mathbf{h}}_{1,u}\|} \right\|, \tag{44}$$

which assumes $\bar{V}_{1,u} \geq \bar{V}_{2,u}$; otherwise, the indices $1, 2$ should be swapped. We can also calculate this beamformer directly

$$\mathbf{f}_u = \sqrt{P_u} \frac{\mathbf{B}_u \bar{\mathbf{h}}_{c_{\max},u}}{\|\mathbf{B}_u \bar{\mathbf{h}}_{c_{\max},u}\|}, \ c_{\max} = \max_{c \in \{1,2\}} \bar{V}_{c,u}. \tag{45}$$

d) SLNR beamforming. Signal to leakage and noise ratio (SLNR) beamforming is a popular coherent beamforming technique for multi-user broadcast and interference channels [59]. If perfect channel state information (CSI) is available at the

transmitters, the SLNR beamformers are obtained by maximizing corresponding Rayleigh quotients involving the instantaneous intended signal and interference leakage powers. However, this is not feasible under the adopted CSIT assumptions of this paper and, similar to [60], we therefore instead consider the expected signal and interference leakage powers, averaged over the unknown diffuse channel components and the random phase shifts of the scattering clusters

$$\text{SLNR}_u = \frac{\mathbb{E}\left(|\mathbf{h}_u^H \mathbf{f}_u|^2\right)}{2\sigma_n^2 + \sum_{j \in \mathcal{S}_g \setminus \{u\}} \mathbb{E}\left(|\mathbf{h}_{j,u}^H \mathbf{f}_u|^2\right)}, \tag{46}$$

$$= \frac{\mathbf{f}_u^H \mathbf{S}_u \mathbf{f}_u}{2\sigma_n^2 + \mathbf{f}_u^H \mathbf{L}_u \mathbf{f}_u}, \tag{47}$$

$$\mathbf{S}_u = \alpha_{1,u}^2 \mathbf{h}_{1,u} \mathbf{h}_{1,u}^H + \alpha_{2,u}^2 \mathbf{h}_{2,u} \mathbf{h}_{2,u}^H + 2\sigma_h^2 \mathbf{I}_{N_t}, \tag{48}$$

$$\mathbf{L}_u = 2\sigma_h^2 (S_g - 1) \mathbf{I}_{N_t}$$
$$+ \sum_{j \in \mathcal{S}_g \setminus \{u\}} \alpha_{1,j,u}^2 \mathbf{h}_{1,j,u} \mathbf{h}_{1,j,u}^H + \alpha_{2,j,u}^2 \mathbf{h}_{2,j,u} \mathbf{h}_{2,j,u}^H. \tag{49}$$

From the intended signal and interference leakage matrices $\mathbf{S}_u$, $\mathbf{L}_u$ the SLNR beamformer is obtained as

$$\mathbf{f}_u = \sqrt{P_u} \max \text{eigvec} \left(\frac{2\sigma_n^2}{P_u} \mathbf{I}_{N_t} + \mathbf{L}_u \right)^{-1} \mathbf{S}_u. \tag{50}$$

e) Robust max-min SINR beamforming. In the spirit of [44]–[46], we perform a robust worst-case expected SINR maximization in the following, where we take the expectation over the diffuse scattering component. Since we generally assume that the diffuse component is weak relative to the two dominant scattering components, the uncertainty in our model is dominated by the multi-path interference of these dominant scatterers and we therefore only consider the worst-case SINR w.r.t. this effect. The worst-case expected SINR of user u is

$$\beta_u^{(\text{wc})} = \frac{p_u^{(\text{wc})} + 2\sigma_h^2}{2\sigma_n^2 + 2\sigma_h^2 (S_g - 1) + \sum_{j \in \mathcal{S}_g \setminus u} p_{u,j}^{(\text{wc})}},$$

$$p_u^{(\text{wc})} = \min_{\boldsymbol{\varphi}_u} \left| (\mathbf{H}_u \boldsymbol{\varphi}_u)^H \mathbf{f}_u \right|^2, \ p_{u,j}^{(\text{wc})} = \max_{\boldsymbol{\varphi}_{u,j}} \left| (\mathbf{H}_{u,j} \boldsymbol{\varphi}_{u,j})^H \mathbf{f}_j \right|^2,$$

$$\mathbf{H}_u = [\alpha_{1,u} \mathbf{h}_{1,u}, \alpha_{2,u} \mathbf{h}_{2,u}], \ \boldsymbol{\varphi}_u = \left[e^{j\varphi_{1,u}}, e^{j\varphi_{2,u}} \right]^H,$$

$$\mathbf{H}_{u,j} = [\alpha_{1,u,j} \mathbf{h}_{1,u,j}, \alpha_{2,u,j} \mathbf{h}_{2,u,j}],$$

$$\boldsymbol{\varphi}_{u,j} = \left[e^{j\varphi_{1,u,j}}, e^{j\varphi_{2,u,j}} \right]^H. \tag{51}$$

With these worst-case SINRs, we can define a robust joint beamformer optimization problem

$$\max_{\mathbf{f}_i, \forall i \in \mathcal{S}_g} \min_{u \in \mathcal{S}_g} \beta_u^{(\text{wc})}$$

subject to

$$\|\mathbf{f}_i\|^2 \leq P_i, \forall i \in \mathcal{S}_g,$$
$$|\boldsymbol{\varphi}_i| = \mathbf{1}, \forall i \in \mathcal{S}_g,$$
$$|\boldsymbol{\varphi}_{i,\ell}| = \mathbf{1}, \forall i, \ell \in \mathcal{S}_g, i \neq \ell. \tag{52}$$

This optimization problem is hard to solve, due to the mutual coupling of interference terms, the product of optimization variables in the power terms $p_u^{(\text{wc})}$ and $p_{u,j}^{(\text{wc})}$, as well as, the unit-modulus constraint of the phase-shift vectors $\boldsymbol{\varphi}_i$ and $\boldsymbol{\varphi}_{i,\ell}$. To simplify the problem, we apply the Cauchy-Schwarz inequality to the interference terms $|(\mathbf{H}_{u,j}\boldsymbol{\varphi}_{u,j})^{\text{H}}\mathbf{f}_j|^2 \leq \|\mathbf{H}_{u,j}\boldsymbol{\varphi}_{u,j}\|^2\|\mathbf{f}_j\|^2 \leq \|\mathbf{H}_{u,j}\boldsymbol{\varphi}_{u,j}\|^2 P_j$ to obtain lower bounds on the worst-case SINRs

$$\beta_u^{(\text{wc})} \geq \beta_u^{(\text{lb})} = \frac{p_u^{(\text{wc})} + 2\sigma_h^2}{2\sigma_n^2 + 2\sigma_h^2\left(S_g - 1\right) + \sum_{j \in \mathcal{S}_g \setminus u} p_{u,j}^{(\text{ub})}},$$

$$p_{u,j}^{(\text{wc})} \leq p_{u,j}^{(\text{ub})} = \max_{\boldsymbol{\varphi}_{u,j}} \left\|\mathbf{H}_{u,j}\boldsymbol{\varphi}_{u,j}\right\|^2 P_j. \quad (53)$$

Now instead of $\beta_u^{(\text{wc})}$, we consider $\beta_u^{(\text{lb})}$ in the optimization in (52). Since $\beta_u^{(\text{lb})}$ is independent of $\mathbf{f}_j$, the beamformer optimization decouples into S_g independent problems. Furthermore, maximizing $\beta_u^{(\text{lb})}$ w.r.t. $\mathbf{f}_u$ reduces to maximizing $p_u^{(\text{wc})}$ and is therefore independent of $\boldsymbol{\varphi}_{u,j}$. We thus obtain the following much simpler optimization problem

$$\max_{\mathbf{f}_u} \min_{\varphi_{1,u},\varphi_{2,u}} \left|\alpha_{1,u}\mathbf{h}_{1,u}^{\text{H}}\mathbf{f}_u e^{j\varphi_{1,u}} + \alpha_{2,u}\mathbf{h}_{2,u}^{\text{H}}\mathbf{f}_u e^{j\varphi_{2,u}}\right|^2. \quad (54)$$

It is easy to see that the minimum is achieved if the two sum-terms are antipodal, leading to

$$\max_{\mathbf{f}_u} \left|\left|\alpha_{1,u}\mathbf{h}_{1,u}^{\text{H}}\mathbf{f}_u\right| - \left|\alpha_{2,u}\mathbf{h}_{2,u}^{\text{H}}\mathbf{f}_u\right|\right|^2. \quad (55)$$

From this equation it is clear that the optimal $\mathbf{f}_u$ has to lie in the 2-dimensional subspace spanned by $\mathbf{H}_u$. We utilize an orthogonal basis $\mathbf{Q}_u \in \mathbb{C}^{N_t \times 2}, \mathbf{Q}_u^{\text{H}}\mathbf{Q}_u = \mathbf{I}_2$ to represent this subspace $\text{span}(\mathbf{Q}_u) = \text{span}(\mathbf{H}_u)$. Hence, we can parametrize the optimal beamformer as $\mathbf{f}_u = \sqrt{P_u}\mathbf{Q}_u[c, \sqrt{1-c^2}e^{j\xi}]^{\text{T}}$, with $c \in [0,1]$ and $\xi \in [0,2\pi]$. By this, the optimization has been reduced to a search over only two parameters, which can easily be solved, e.g., by a two-dimensional grid-search.

REFERENCES

[1] S. Schwarz, B. R. Elbal, E. Z6chmann, L. Marijanovic, and S. Pratschner, "Dependable wireless connectivity: Insights and methods for 5G and beyond," *E&I Elektrotechnik Und Informationstechnik*, vol. 135, pp. 449–455, 2018.

[2] F. Foukalas, P. Pop, F. Theoleyre, C. A. Boano, and C. Buratti, "Dependable wireless industrial IoT networks: Recent advances and open challenges," in *Proc. IEEE Euro. Test Symp.*, 2019, pp. 1–10.

[3] O. Semiari, W. Saad, M. Bennis, and M. Debbah, "Integrated millimeter wave and sub-6 GHz wireless networks: A roadmap for joint mobile broadband and ultra-reliable low-latency communications," *IEEE Wireless Commun.*, vol. 26, no. 2, pp. 109–115, Apr. 2019.

[4] J. Yang *et al.*, "Ultra-reliable communications for industrial internet of things: Design considerations and channel modeling," *IEEE Netw.*, vol. 33, no. 4, pp. 104–111, Jul./Aug. 2019.

[5] A. Azari, M. Ozger, and C. Cavdar, "Risk-aware resource allocation for URLLC: Challenges and strategies with machine learning," *IEEE Commun. Mag.*, vol. 57, no. 3, pp. 42–48, Mar. 2019.

[6] E. Khorov, A. Krasilov, I. Selnitsky, and I. Akyildiz, "A framework to maximize the capacity of 5G systems for ultra-reliable low-latency communications," *IEEE Trans. Mobile Comput.*, to be published, doi: 10.1109/TMC.2020.2976055.

[7] D. Feng *et al.*, "Toward ultrareliable low-latency communications: Typical scenarios, possible solutions, and open issues," *IEEE Veh. Technol. Mag.*, vol. 14, no. 2, pp. 94–102, Jun. 2019.

[8] H. Ji, S. Park, J. Yeo, Y. Kim, J. Lee, and B. Shim, "Ultra-reliable and low-latency communications in 5G downlink: Physical layer aspects," *IEEE Wireless Commun.*, vol. 25, no. 3, pp. 124–130, Jun. 2018.

[9] G. Dong, H. Zhang, S. Jin, and D. Yuan, "Energy-efficiency-oriented joint user association and power allocation in distributed massive MIMO systems," *IEEE Trans. Veh. Technol.*, vol. 68, no. 6, pp. 5794–5808, Jun. 2019.

[10] S. Schwarz and S. Pratschner, "Dynamic distributed antenna systems with wireless mmWave fronthaul," in *Proc. 53rd Annu. Asilomar Conf. Signals, Syst., Comput.*, 2019, pp. 1–7.

[11] J. Zhang, S. Chen, Y. Lin, J. Zheng, B. Ai, and L. Hanzo, "Cell-free massive MIMO: A new next-generation paradigm," *IEEE Access*, vol. 7, pp. 99 878–99 888, 2019.

[12] E. Björnson and L. Sanguinetti, "Scalable cell-free massive MIMO systems," *IEEE Trans. Commun.*, vol. 68, no. 7, pp. 4247–4261, Jul. 2020.

[13] B. P. S. Sahoo, C. Chou, C. Weng, and H. Wei, "Enabling millimeter-wave 5G networks for massive IoT applications: A closer look at the issues impacting millimeter-waves in consumer devices under the 5G framework," *IEEE Consum. Electron. Mag.*, vol. 8, no. 1, pp. 49–54, 2019.

[14] G. Kwon and H. Park, "Joint user association and beamforming design for millimeter wave UDN with wireless backhaul," *IEEE J. Sel. Areas Commun.*, vol. 37, no. 12, pp. 2653–2668, Dec. 2019.

[15] K. Yang, N. Yang, N. Ye, M. Jia, Z. Gao, and R. Fan, "Non-orthogonal multiple access: Achieving sustainable future radio access," *IEEE Commun. Mag.*, vol. 57, no. 2, pp. 116–121, Feb. 2019.

[16] M. Elbayoumi, M. Kamel, W. Hamouda, and A. Youssef, "NOMA-assisted machine-type communications in UDN: State-of-the-art and challenges," *IEEE Commun. Surv. Tut.*, vol. 22, no. 2, pp. 1276-1304, Secondquarter 2020.

[17] G. Song, W. Wang, D. Chen, and T. Jiang, "KPI/KQI-driven coordinated multipoint in 5G: Measurements, field trials, and technical solutions," *IEEE Wireless Commun.*, vol. 25, no. 5, pp. 23–29, Oct. 2018.

[18] M. S. Ali, E. Hossain, and D. I. Kim, "Coordinated multipoint transmission in downlink multi-cell NOMA systems: Models and spectral efficiency performance," *IEEE Wireless Commun.*, vol. 25, no. 2, pp. 24–31, Apr. 2018.

[19] S. Chen, T. Zhao, H. Chen, and W. Meng, "Downlink coordinated multi-point transmission in ultra-dense networks with mobile edge computing," *IEEE Netw.*, vol. 33, no. 2, pp. 152–159, Mar./Apr. 2019.

[20] Q. Nadeem, A. Kammoun, and M. Alouini, "Elevation beamforming with full dimension MIMO architectures in 5G systems: A tutorial," *IEEE Commun. Surveys Tut.*, vol. 21, no. 4, pp. 3238–3273, Fourthquarter 2019.

[21] 3GPP, "TSG RAN; Study on channel model for frequencies from 0.5 to 100 GHz (release 16)," Dec. 2019, [Online]. Available: http://www.3gpp.org/DynaReport/38901.htm

[22] F. Ademaj, S. Schwarz, T. Berisha, and M. Rupp, "A spatial consistency model for geometry-based stochastic channels," *IEEE Access*, vol. 7, pp. 183 414–183 427, 2019.

[23] S. Jaeckel, L. Raschkowski, K. Börner, and L. Thiele, "Quadriga: A 3-D multi-cell channel model with time evolution for enabling virtual field trials," *IEEE Trans. Antennas Propag.*, vol. 62, no. 6, pp. 3242–3256, Jun. 2014.

[24] S. Schwarz, E. Zöchmann, M. M, and K. Guan, "Dependability of directional millimeter wave vehicle-to-infrastructure communications," *IEEE Access*, vol. 8, pp. 53 162–53 171, Mar. 2020.

[25] E. Zöchmann *et al.*, "Better than rician: Modelling millimetre wave channels as two-wave with diffuse power," *EURASIP J. Wireless Commun. Netw.*, vol. 2019, no. 1, pp. 1–17, Jan. 2019.

[26] E. Zöchmann, J. Blumenstein, R. Marsalek, M. Rupp, and K. Guan, "Parsimonious channel models for millimeter wave railway communications," in *Proc. IEEE Wireless Commun. Netw. Conf.*, 2019, pp. 1–6.

[27] S. Schwarz, "Outage investigation of beamforming over random-phase finite-scatterer MISO channels," *IEEE Signal Process. Lett.*, vol. 24, no. 7, pp. 1029–1033, Jul. 2017.

[28] G. D. Durgin, T. S. Rappaport, and D. A. de Wolf, "New analytical models and probability density functions for fading in wireless communications," *IEEE Trans. Commun.*, vol. 50, no. 6, pp. 1005–1015, Jun. 2002.

[29] M. Rao, F. J. Lopez-Martinez, and A. Goldsmith, "Statistics and system performance metrics for the two wave with diffuse power fading model," in *Proc. Conf. Infor. Sci. Syst.*, 2014, pp. 1–6.

[30] S. H. Oh, K. H. Li, and W. S. Lee, "Performance of BPSK pre-detection MRC systems over two-wave with diffuse power fading channels," *IEEE Trans. Wireless Commun.*, vol. 6, no. 8, pp. 2772–2775, Aug. 2007.

[31] Y. Lu, X. Wang, and N. Yang, "Outage probability of cooperative relay networks in two-wave with diffuse power fading channels," *IEEE Trans. Commun.*, vol. 60, no. 1, pp. 42–47, Jan. 2012.

[32] N. Y. Ermolova, "Capacity analysis of two-wave with diffuse power fading channels using a mixture of gamma distributions," *IEEE Commun. Lett.*, vol. 20, no. 11, pp. 2245–2248, Nov. 2016.

[33] E. Chatziantoniou, B. Allen, V. Velisavljevic, P. Karadimas, and J. Coon, "Energy detection based spectrum sensing over two-wave with diffuse power fading channels," *IEEE Trans. Veh. Technol.*, vol. 66, no. 1, pp. 868–874, Jan. 2017.

[34] H. Meinel and A. Plattner, "Millimetre-wave propagation along railway lines," *IEE Proc. F—Commun., Radar Signal Process.*, vol. 130, no. 7, pp. 688–694, 1983.

[35] V. Va, T. Shimizu, G. Bansal, and R. W. H. Jr., "Millimeter wave vehicular communications: A survey," *Foundations Trends Netw.*, vol. 10, no. 1, pp. 1–113, 2016.

[36] *5G Americas*, "The 5G evolution: 3GPP releases 16-17," white paper, Jan. 2020. [Online]. Available: https://www.5gamericas.org/5g-evolution-3gpp-releases-16-17/

[37] J. Choi, V. Va, N. Gonzalez-Prelcic, R. Daniels, C. R. Bhat, and R. W. Heath, "Millimeter-wave vehicular communication to support massive automotive sensing," *IEEE Commun. Mag.*, vol. 54, no. 12, pp. 160–167, Dec. 2016.

[38] R. Deng, B. Di, and L. Song, "Cooperative collision avoidance for overtaking maneuvers in cellular V2X-based autonomous driving," *IEEE Trans. Veh. Technol.*, vol. 68, no. 5, pp. 4434–4446, May 2019.

[39] R. Ford, M. Zhang, M. Mezzavilla, S. Dutta, S. Rangan, and M. Zorzi, "Achieving ultra-low latency in 5G millimeter wave cellular networks," *IEEE Commun. Mag.*, vol. 55, no. 3, pp. 196–203, Mar. 2017.

[40] Y. Yang, Z. Gao, Y. Ma, B. Cao, and D. He, "Machine learning enabling analog beam selection for concurrent transmissions in millimeter-wave V2V communications," *IEEE Trans. Veh. Technol.*, vol. 69, no. 8, pp. 9185–9189, Aug. 2020.

[41] F. Liu, C. Masouros, A. P. Petropulu, H. Griffiths, and L. Hanzo, "Joint radar and communication design: Applications, state-of-the-art, and the road ahead," *IEEE Trans. Commun.*, vol. 68, no. 6, pp. 3834–3862, Jun. 2020.

[42] S. Schwarz and M. Rupp, "Dependability enhancements for transmission over MISO TWDP fading channels," in *Proc. IEEE Int. Workshop Signal Process. Adv. Wireless Commun.*, 2020, pp. 1–5.

[43] K. Wang, T. Chang, W. Ma, A. M. So, and C. Chi, "Probabilistic SINR constrained robust transmit beamforming: A bernstein-type inequality based conservative approach," in *Proc. IEEE Int. Conf. Acoust., Speech Signal Process.*, 2011, pp. 3080–3083.

[44] A. Tajer, N. Prasad, and X. Wang, "Robust linear precoder design for multi-cell downlink transmission," *IEEE Trans. Signal Process.*, vol. 59, no. 1, pp. 235–251, Jan. 2011.

[45] E. Björnson, G. Zheng, M. Bengtsson, and B. Ottersten, "Robust monotonic optimization framework for multicell MISO systems," *IEEE Trans. Signal Process.*, vol. 60, no. 5, pp. 2508–2523, May 2012.

[46] C. Shen, T. Chang, K. Wang, Z. Qiu, and C. Chi, "Distributed robust multi-cell coordinated beamforming with imperfect CSI: An ADMM approach," *IEEE Trans. Signal Process.*, vol. 60, no. 6, pp. 2988–3003, Jun. 2012.

[47] E. Zöchmann *et al.*, "Position-specific statistics of 60 GHz vehicular channels during overtaking," *IEEE Access*, vol. 7, pp. 14 216–14 232, 2019.

[48] T. Rappaport *et al.*, "Millimeter wave mobile communications for 5G cellular: It will work!," *IEEE Access*, vol. 1, pp. 335–349, 2013.

[49] M. R. Akdeniz *et al.*, "Millimeter wave channel modeling and cellular capacity evaluation," *IEEE J. Sel. Areas Commun.*, vol. 32, no. 6, pp. 1164–1179, Jun. 2014.

[50] D. He *et al.*, "Channel measurement, simulation, and analysis for high-speed railway communications in 5G millimeter-wave band," *IEEE Trans. Intell. Transp. Syst.*, vol. 19, no. 10, pp. 3144–3158, Oct. 2018.

[51] H. Groll *et al.*, "Sparsity in the delay-doppler domain for measured 60 GHz vehicle-to-infrastructure communication channels," in *Proc. IEEE Int. Conf. Commun. Workshops*, May 2019, pp. 1–6.

[52] R. W. Heath, N. Gonzllez-Prelcic, S. Rangan, W. Roh, and A. M. Sayeed, "An overview of signal processing techniques for millimeter wave MIMO systems," *IEEE J. Sel. Top. Signal Process.*, vol. 10, no. 3, pp. 436–453, Apr. 2016.

[53] S. Rangan, T. Rappaport, and E. Erkip, "Millimeter-wave cellular wireless networks: Potentials and challenges," *Proc. IEEE*, vol. 102, no. 3, pp. 366–385, Mar. 2014.

[54] M. Rao, F. J. Lopez-Martinez, M. S. Alouini, and A. Goldsmith, "MGF approach to the analysis of generalized two-ray fading models," *IEEE Trans. Wireless Commun.*, vol. 14, no. 5, pp. 2548–2561, May 2015.

[55] D. A. Bodenham and N. M. Adams, "A comparison of efficient approximations for a weighted sum of chi-squared random variables," *Stat. Comput.*, vol. 26, pp. 917–928, 2016.

[56] J. Nocedal and S. J. Wright, *Numerical Optimization*, 2nd ed. Berlin, Germany: Springer, 2006.

[57] E. T. Bell, "Exponential numbers," *The Amer. Math. Monthly*, vol. 41, no. 7, pp. 411–419, 1934.

[58] J. M. Romero-Jerez, F. J. Lopez-Martinez, J. P. Peña-Martìn, and A. Abdi, "Stochastic fading channel models with multiple dominant specular components for 5G and beyond," *Arxiv,vol.abs/1905.03567*.

[59] M. Sadek, A. Tarighat, and A. Sayed, "A leakage-based precoding scheme for downlink multi-user MIMO channels," *IEEE Trans. Wireless Commun.*, vol. 6, no. 5, pp. 1711–1721, May 2007.

[60] S. Schwarz, "Robust full-dimension MIMO transmission based on limited feedback angular-domain CSIT," *EURASIP J. Wireless Commun. Netw.*, vol. 2018, no. 1, pp. 1–20, Mar. 2018.

Stefan Schwarz (Senior Member, IEEE) received the Dr. Techn. degree (Ph.D. equivalent) in telecommunications engineering from the Technical University of Vienna (TU Wien), Austria, in 2013. He currently holds a Tenure Track position as an Assistant Professor with the Institute of Telecommunications, TU Wien, where he also heads the Christian Doppler Laboratory for Dependable Wireless Connectivity for the Society in Motion. His research interests include wireless communications, signal processing, and channel modeling. He is an Associate Editor of IEEE ACCESS and *EURASIP JWCN*.

Markus Rupp (Fellow, IEEE) received the Dipl. Ing. degree from the University of Saarbrücken, Germany, in 1988, and the Dr. Ing. degree from Technische Universität Darmstadt, Germany, in 1993. Until 1995, he held a Postdoctoral position with the University of California at Santa Barbara, Santa Barbara, CA, USA. From 1995 to 2001, he was with the Wireless Technology Research Department, Bell Labs, Holmdel, NJ, USA. Since 2001, he has been a Full Professor of digital signal processing in mobile communications with TU Wien.